Representation of Truck Tire Properties
In Braking and Handling Studies:
The Influences of Vertical Load on
Side Force Characteristics
UMTRI, August 1988

EDC Library Ref. No. 1089

TRI-88-29

REPRESENTATION OF TRUCK TIRE PROPERTIES IN AKING AND HANDLING STUDIES: THE INFLUENCES OF VERTICAL LOAD ON SIDE FORCE CHARACTERISTICS

MVMA Project No. 8168

Luis Balderas
Paul Fancher

August 1988

UMTRI The University of Michigan Transportation Research Institute

UMTRI

Technical Report Documentation Page

1. Report No.	2. Government Accession No. PB89 143002 AS	3. Recipient's Catalog No. 776631
4. Title and Subtitle REPRESENTATION OF TRUCK TIRE PROPERTIES IN BRAKING AND HANDLING STUDIES: THE INFLUENCE OF VERTICAL LOAD ON SIDE FORCE CHARACTERISTICS		5. Report Date August 1988
		6. Performing Organization Code
7. Author(s) Luis Balderas, Paul Fancher		8. Performing Organization Report No. UMTRI-88-29
9. Performing Organization Name and Address The University of Michigan Transportation Research Institute 2901 Baxter Road, Ann Arbor, Michigan 48109		10. Work Unit No. (TRAIS)
		11. Contract or Grant No. MVMA Proj. 8168
12. Sponsoring Agency Name and Address Motor Vehicle Manufacturers Association 300 New Center Building Detroit, Michigan 48202		13. Type of Report and Period Covered Final 7/87-8/88
		14. Sponsoring Agency Code
15. Supplementary Notes		

16. Abstract

A semi-empirical tire model has been augmented to represent the manner in which both the cornering stiffness and pressure distribution change with vertical load. Model predictions and test data are compared to illustrate the influences of cornering stiffness and pressure distribution on the shear force properties of truck tires.

The enhanced representation of side force capability has been incorporated into a model for predicting traction fields under conditions of combined longitudinal and lateral slip.

17. Key Words tire shear force, traction fields for truck tires, tire modeling	18. Distribution Statement UNLIMITED

19. Security Classif. (of this report)	20. Security Classif. (of this page)	21. No. of Pages	22. Price
NONE	NONE	51	

TABLE OF CONTENTS

NOMENCLATURE

Symbol	Definition
a	Length of the increasing and decreasing pressure zones (see Figure 1)
C	General symbol used in representing any tire parameter (see page 29)
C_α	Cornering stiffness, lb/deg
C_S	Longitudinal stiffness, lb/unit slip
μ_y	Lateral frictional coupling
μ_x	Longitudinal frictional coupling
μ_0	Combined frictional coupling value
μ	Frictional coupling
a/l or a/L	Pressure distribution parameter
X_P	Pneumatic trail, inches
C_y	Lateral deflection stiffness, lb/in
A_S	Friction reduction factor, sec/ft
V_S	Sliding velocity, ft/sec
u_w	Longitudinal velocity of the tire, mph
α	Slip angle, degrees
S_x	Longitudinal slip
F_Z	Vertical tire load, lb
F_{Z0}	Nominal tire load, lb
V	Test velocity, mph
V_0	Nominal tire velocity, mph
L or l	Length of the contact patch
W	Width of the contact patch

x_s	Longitudinal location of the sliding boundary
P_{max}	Maximum pressure value in the contact patch
F_X	Longitudinal tire braking force, lb
E	Denotes scientific notation
F_Y	Lateral tire force, lb
θ	Angle between the sliding direction and the tire undeformed center line
A_T	Aligning torque, in-lbs
X^2	Statistical chi square (defined on page 3)

1.0 INTRODUCTION

UMTRI's existing tire model has been revised during 1988 to improve the prediction of side force under conditions when the vertical load is changing drastically, such as in turns approaching the rollover thresholds of trucks or in sudden obstacle-avoidance maneuvers. This work was completed as part of a research program supported by the Motor Vehicle Manufacturers Association. The overall objective of this program is to provide semi-empirical models for representing the influences of operating conditions on the lateral and longitudinal shear forces generated by truck tires.

The shear force characteristics of truck tires are highly dependent upon vertical load, tread wear, pavement texture, and water depth. Information available from a limited amount of testing has been used by UMTRI to estimate the influences of tread wear and pavement texture on the levels of tire/road friction applicable for braking on wet surfaces [1]. In addition, we have observed that vertical load has an important influence on the side force characteristics of truck tires [2,3]. The results of these activities indicate that improved tire traction models are needed to allow greater flexibility and to provide more accurate estimates of shear forces for extrapolating to vehicle operating conditions for which analysts may only have limited amounts of test data for truck tires.

Based on the preferences of the MVMA Medium and Heavy Truck Performance Panel, we have addressed the influences of vertical load on side force characteristics during this past year. Work on factors influencing levels of tire/road friction will receive attention next year.

After providing background information on the semi-empirical tire model, the report presents results obtained by using the model to study data measured for two types of radial truck tires. Then the model is used to predict traction fields covering situations in which the tire is subjected to both longitudinal and lateral slip. A concluding section discusses connections between this tire model and future experimental and analytical studies pertaining to tires and vehicles. The equations for the model are presented in Appendix A. Additional information concerning the computation of traction fields is presented in Appendix B.

2.0 BACKGROUND ON THE TIRE MODEL

A Tire Model for Combined Steering and Braking Maneuvers

This section gives a brief description of the semi-empirical tire model used in this study.

The most important assumptions of the model are:

1) The pressure distribution can be approximated by a trapezoidal shape along the length of the contact patch (see Figure 1). (Variations in pressure across the width of the contact patch are averaged together. Hence, the lateral distribution of pressure does not appear in the analysis.)

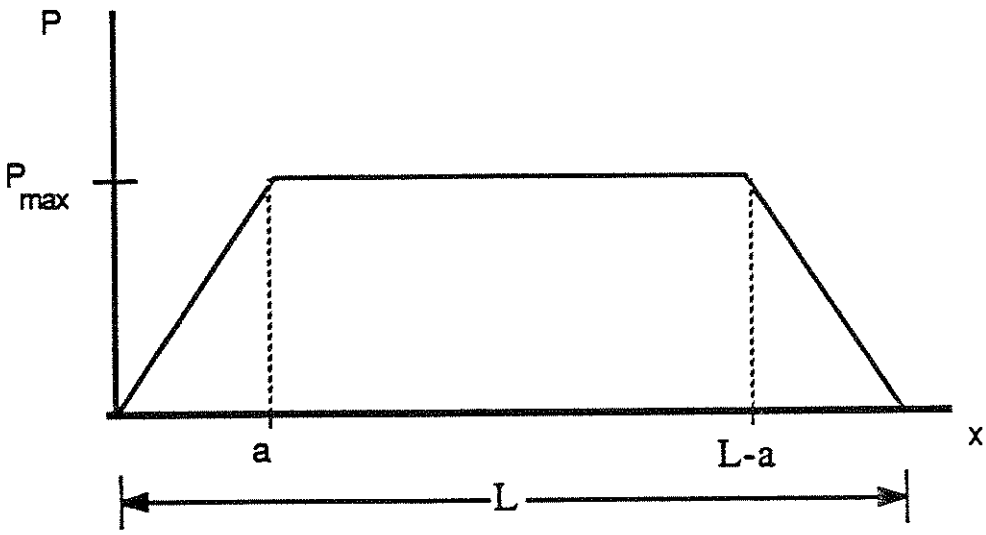

where:

$$P_{max} = \frac{|F_z|}{(L-a) * W}$$

L = length of the contact patch
W = width of the contact patch
a = length of the increasing and decreasing pressure zones

Figure 1. Approximation to the pressure distribution over the contact patch.

2) The contact patch can be divided into sliding and adhesive zones. (The boundary between the sliding and cornering zones is denoted by the symbol x_s.)

3) The longitudinal force, F_x, and the lateral force, F_y, are obtained by integrating the shear stress over the contact patch. Because of the form of the pressure distribution, there are three different regions where x_s may be found. These regions are:

   a) Decreasing pressure region, $L\text{-}a < x_s \leq L$

   b) Central region of pressure distribution, $a < x_s \leq L\text{-}a$

   c) Increasing pressure region, $0.0 \leq x_s \leq a$ (Here, the entire contact patch is sliding and there is no adhesion region in the contact patch.)

The results of the integrations are given on Appendix A.

4) The shear stresses in the adhesion zone of the contact patch are determined by the elastic properties of the tire. (The quantity C_α, the cornering stiffness, represents the influence of

lateral elastic properties of the tire and C_s, the longitudinal (or circumferential) stiffness, represents the longitudinal elastic properties of the tire.)

5) The shear stresses in the sliding zone of the contact patch are determined by the frictional properties of the tire/road interface. (The friction level may vary with normal load, speed, and other factors.)

These assumptions are typical of those used in developing semi-empirical tire models. See References [4 and 5]. The new features of this model are the introductions of second-order polynomials to represent the changes in (the basic quantities describing the tire) a/L, C_α, and μ, as brought about by changes in vertical load. In particular, the notion that the form of the pressure distribution (as controlled by a/L) changes as vertical load changes is a new idea. In the next section, tire data are examined to develop quantitative results for the influences of vertical load on the basic quantities (a/L, C_α, and μ) describing tires.

3.0 PROCESSING OF TIRE DATA

Description of the Computer Algorithm for Processing Tire Data

The data processing algorithm determines the lateral parameters (C_α, μ_y and a/L) for the tire model using lateral force data such as that obtained from the UMTRI flat-bed tire test machine. This algorithm uses the Levenberg-Marquardt method for nonlinear models [6]. The Marquardt method is a statistical algorithm that, given a set of initial values for the parameters, makes use of the gradient and a factor to accelerate the convergence of the fit minimizing the value of the sum of the squares of the errors (X^2).

The algorithm has the flexibility of keeping some of the parameters fixed and then finding the best fit for the others. Furthermore, the program can be used to study the deviation and effects of the variations of tire parameters from the best fitted values. Examples of these types of results are presented later in this section.

Assumptions Made in Processing Tire Data

The main assumptions made in applying the data processing algorithm were:

1 - The longitudinal properties, C_s and μ_x, were not included; therefore, the only parameters to be fitted were C_α, μ_y and a/l.

2 - The sliding velocity, Vs, is almost nil. This means that in Equations 1 and 3 of Appendix A the following relationship applies:

$$\mu_y = \mu_0 \approx \mu$$

Note that this approximation is only valid for low test speeds and small angles.

Examples of Fitted Data

Six tires were studied in this project. The data for these tires were available at the time this study was performed. The tires were tested on the UMTRI flatbed tire tester [7] at five different loads and six different slip angles. To obtain the input data required by the program, the results of the experiments were averaged beforehand and then fed to the computer. The list of the experimental tires is given below.

Tire No	Type	Description
1	Michelin 11/80 R22.5 Pilote	Full Tread
2	Michelin 11/80 R22.5 Pilote	Full Tread
3	Michelin 11R22.5 XZA	Full Tread
4	Michelin 11R22.5 XZA	Full Tread
5	Michelin 11R22.5 XZA	Half Tread
6	Michelin 11R22.5 XZA	1/3 Tread

Since the quality of fit was comparable for all six tires, fitted values obtained for three of these tires, tires #1, 3 and 6, are presented below to illustrate the match between measured and fitted results for different tires. Parametric values for all six tires are presented in the next section.

TIRE # 1, MICHELIN 11/80 R22.5, FULL TREAD.

The results of the fitting process for the five different loads are presented in Figures 2 through 6. The experimental points are depicted by the dots, and the solid line represents the curve generated by the model using the results for the best fit found for that particular load.

The variables plotted are the slip angle, α, in degrees along the abscissa, and the ratio of lateral force, F_Y, to normal load, F_Z, along the ordinate.

The results of the fit are also presented in tabular form below each graph. The second and third columns in these tabulations contain the values of the experimental force and the force estimated by the model for each slip angle shown in the first column. The right-most column represents the percentage difference between these two forces.

Examination of the results presented in Figures 2 through 6 show that a good fit is obtained for this tire with an average overall error of approximately 1.05%.

TIRE # 3, MICHELIN 11R22.5, FULL TREAD.

The results of the fitting process for this tire are presented in Figures 7 through 11.

A better fit is obtained as normal load increases, especially for the upper ends of the curves. The standard error decreases considerably for high loads.

In general, a good fit is obtained for this tire with an average overall error of about 1.09%.

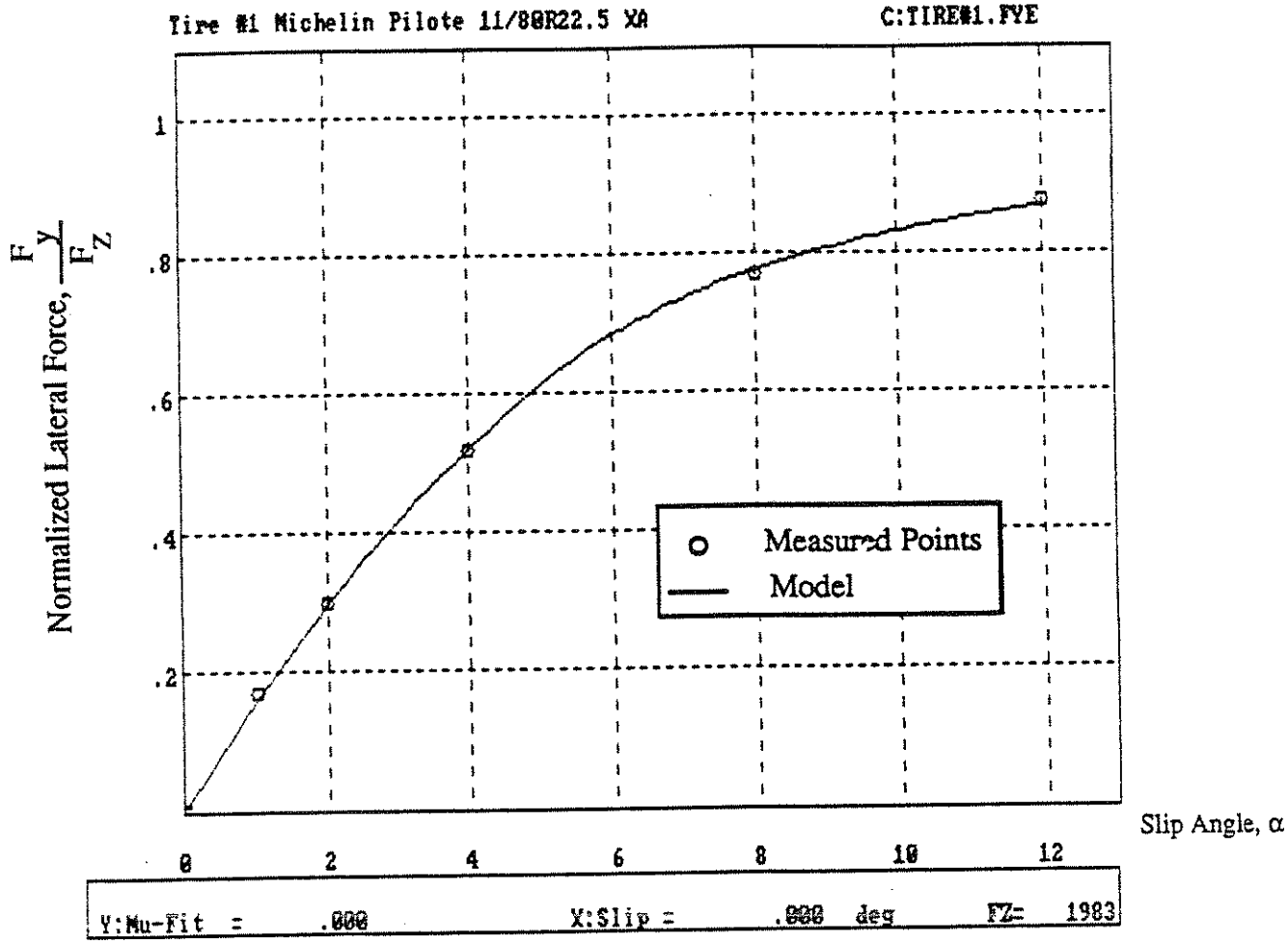

Table of Results
Vertical Load = 1983.07 lbs
Calfa = 342.60 Lb/deg
Mu = .8686
a/l = .2931

Slip Ang. (deg)	Fy (exp.) lb.	Fy (fitted) lb.	%CH
1.00	335.40	316.53	-5.6254
2.00	592.21	588.42	-.6400
4.00	1029.62	1031.85	.2163
8.00	1524.40	1541.54	1.1244
12.00	1734.79	1722.52	-.7073

X^2 = 819.6696

Figure 2. Results for Tire #1 at 1983 lbs

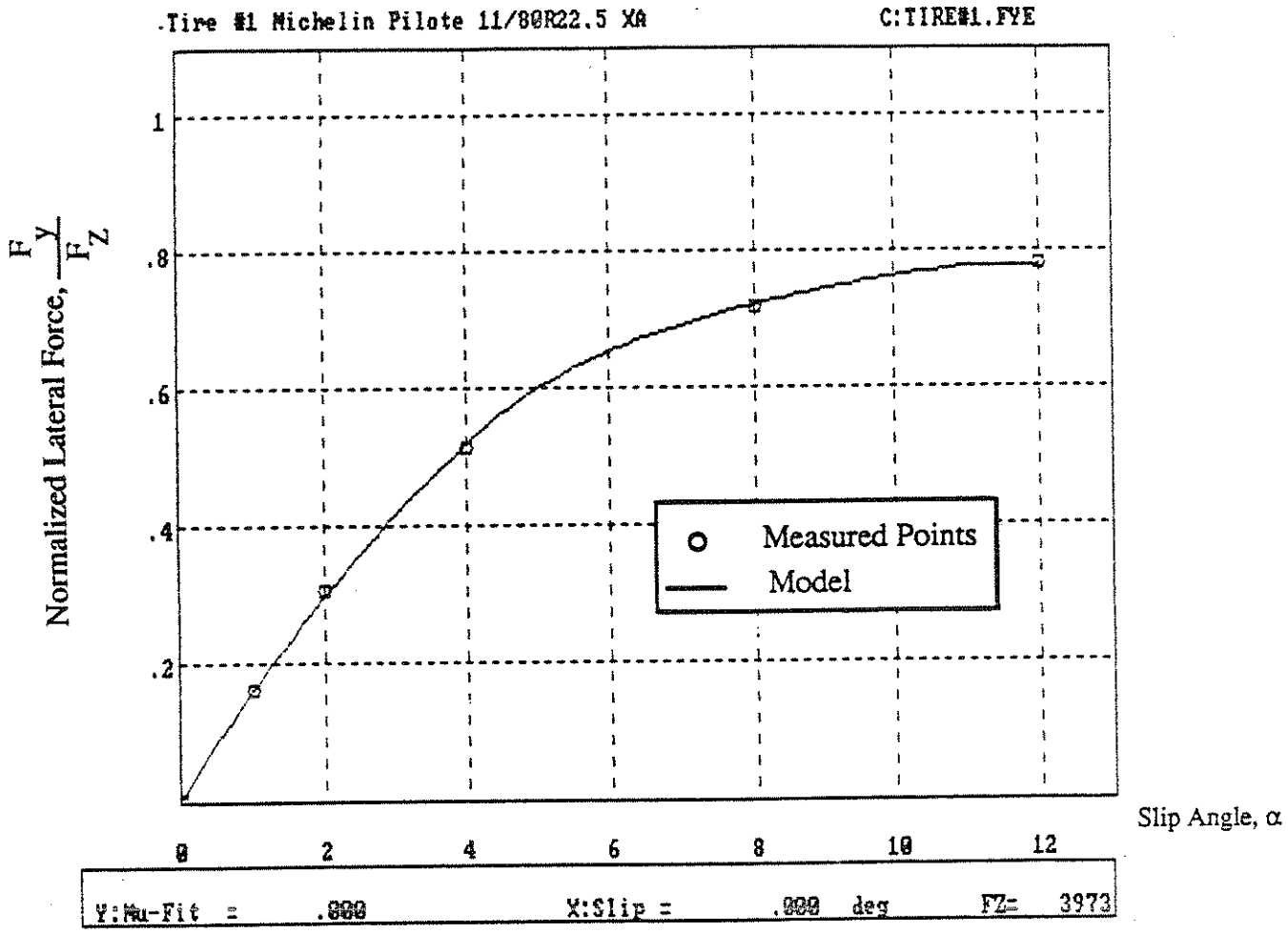

Table of Results
Vertical Load = 3973.58 lbs
Calfa = 699.53 Lb/deg
Mu = .7796
a/l = .2687

Slip Ang. (deg)	Fy (exp.) lb.	Fy (fitted) lb.	%CH
1.00	645.87	642.56	-.5132
2.00	1216.60	1188.55	-2.3054
4.00	2052.58	2067.49	.7263
8.00	2861.00	2870.45	.3304
12.00	3104.98	3097.72	-.2338

X^2 = 1161.9980

Figure 3. Results for Tire #1 at 3973 lbs

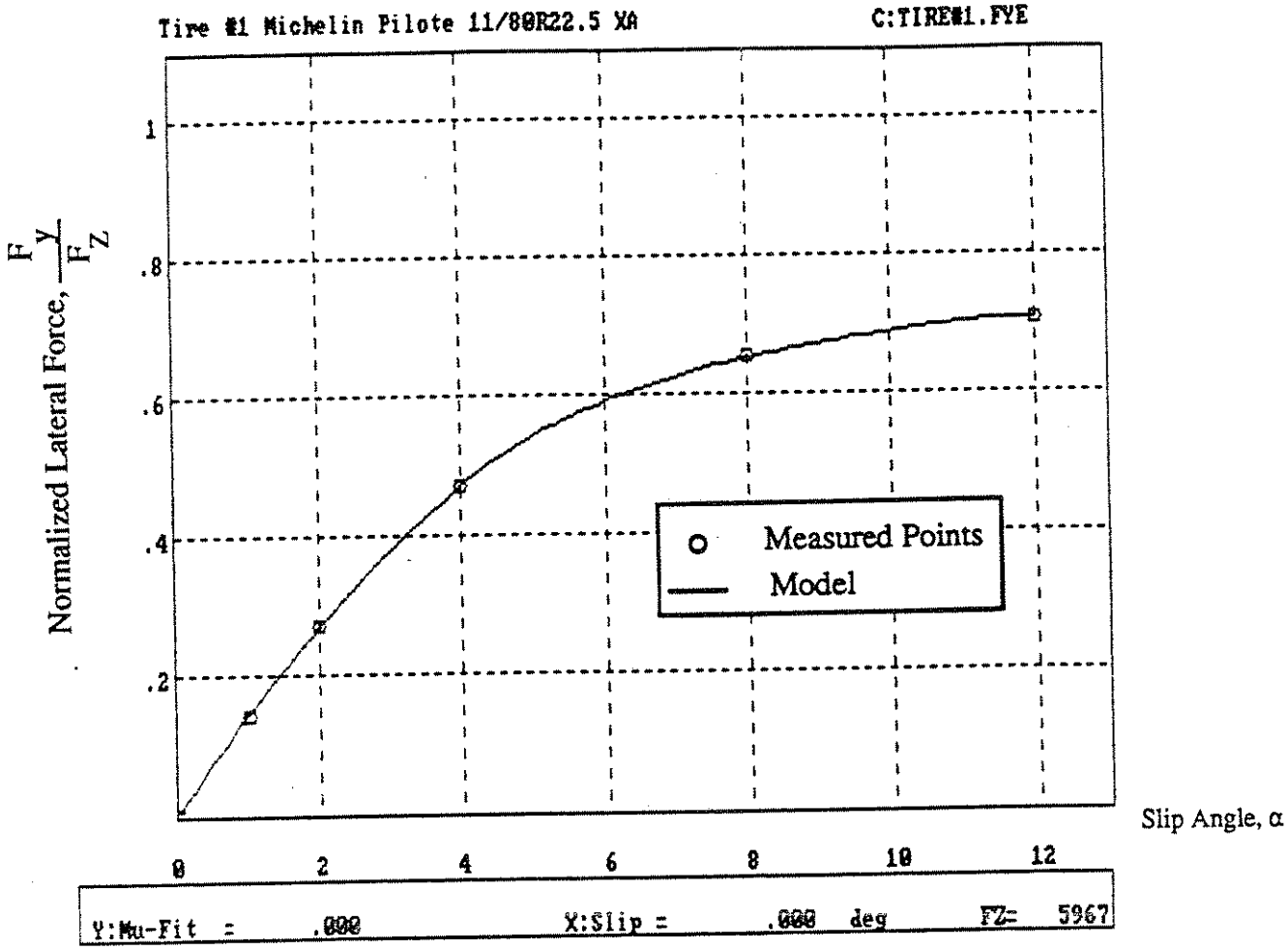

Table of Results
Vertical Load = 5967.33 lbs
Calfa = 945.21 Lb/deg
Mu = .7074
a/l = .2632

Slip Ang. (deg)	Fy (exp.) lb.	Fy (fitted) lb.	%CH
1.00	833.77	869.75	4.3149
2.00	1609.67	1611.19	.0946
4.00	2818.93	2809.42	-.3375
8.00	3907.27	3897.02	-.2624
12.00	4213.41	4221.21	.1852

X^2 = 1553.0790

Figure 4. Results for Tire #1 at 5967 lbs

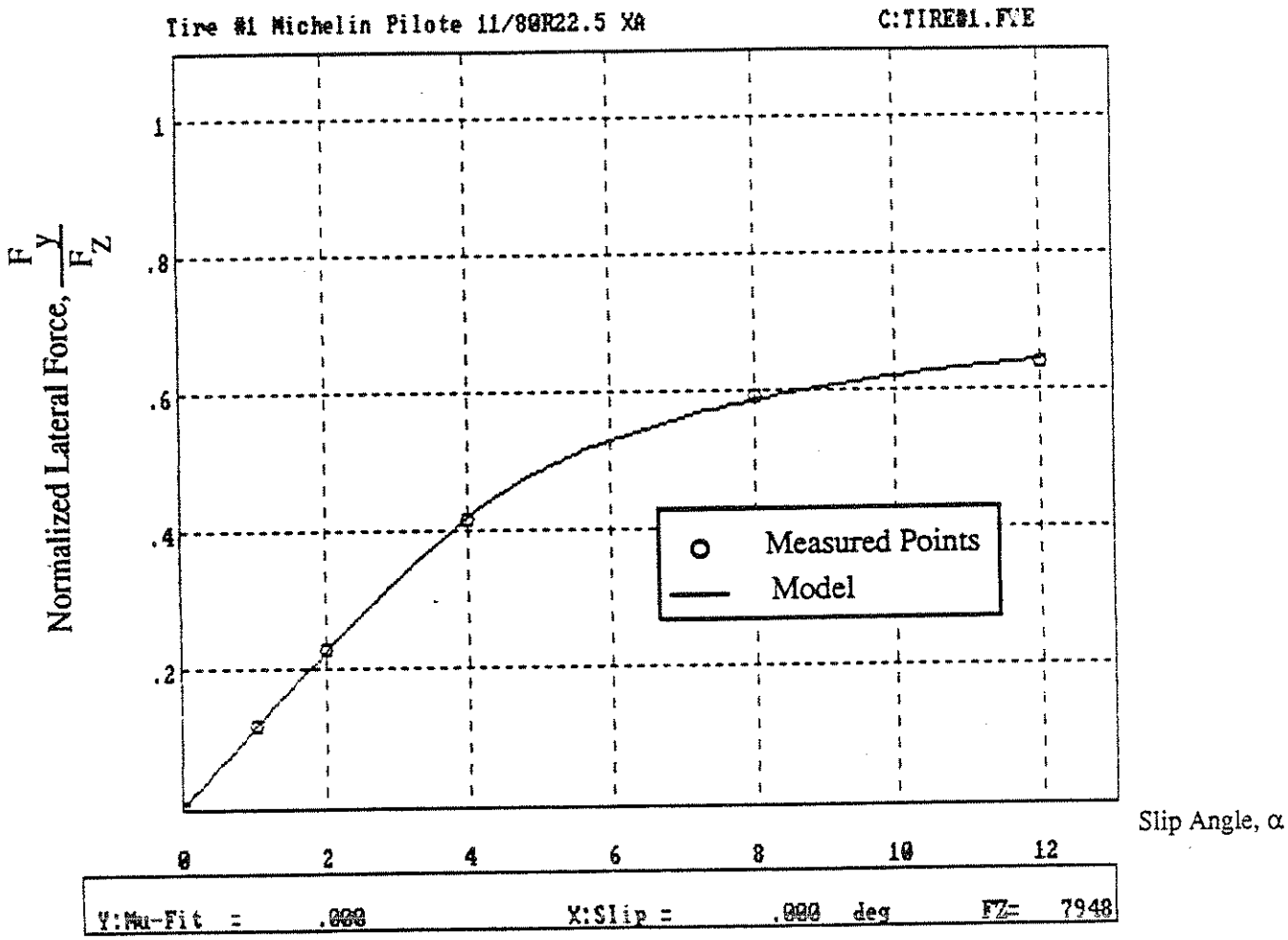

Table of Results
Vertical Load = 7948.79 lbs
Calfa = 978.63 Lb/deg
Mu = .6950
a/l = .1473

Slip Ang. (deg)	Fy (exp.) lb.	Fy (fitted) lb.	%CH
1.00	924.09	937.01	1.3976
2.00	1808.67	1797.92	-.5944
4.00	3308.71	3325.17	.4976
8.00	4726.41	4670.17	-1.1899
12.00	5079.43	5121.43	.8269

X^2 = 5480.3320

Figure 5. Results for Tire #1 at 7948 lbs

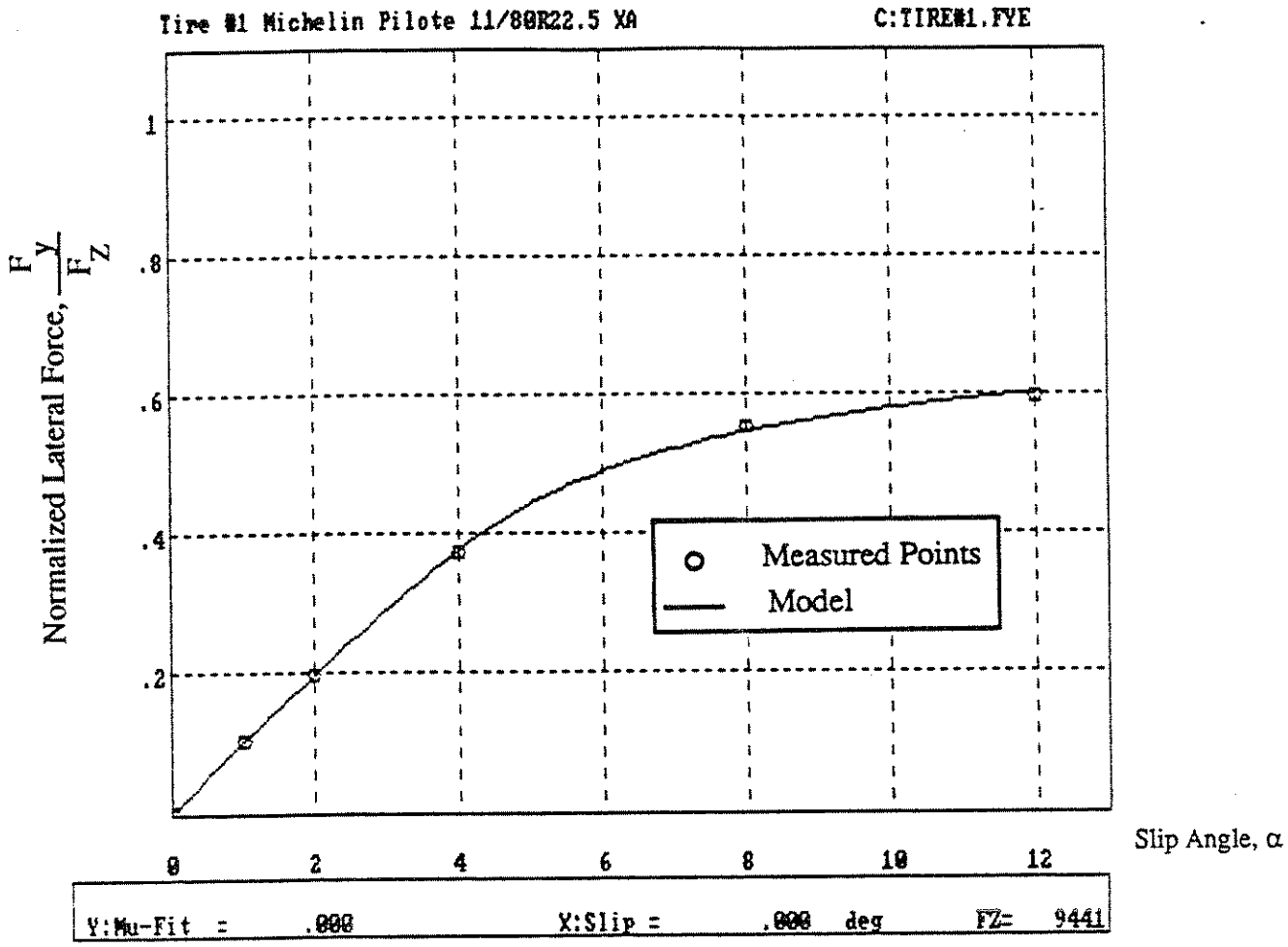

Table of Results
Vertical Load = 9441.42 lbs
Calfa = 982.87 Lb/deg
Mu = .6781
a/l = .0980

Slip Ang. (deg)	Fy (exp.) lb.	Fy (fitted) lb.	%CH
1.00	947.68	956.96	.9795
2.00	1872.50	1865.17	-.3915
4.00	3533.32	3551.45	.5131
8.00	5225.22	5158.43	-1.2782
12.00	5647.58	5697.59	.8855

X^2 = 7430.2810

Figure 6. Results for Tire #1 at 9441 lbs

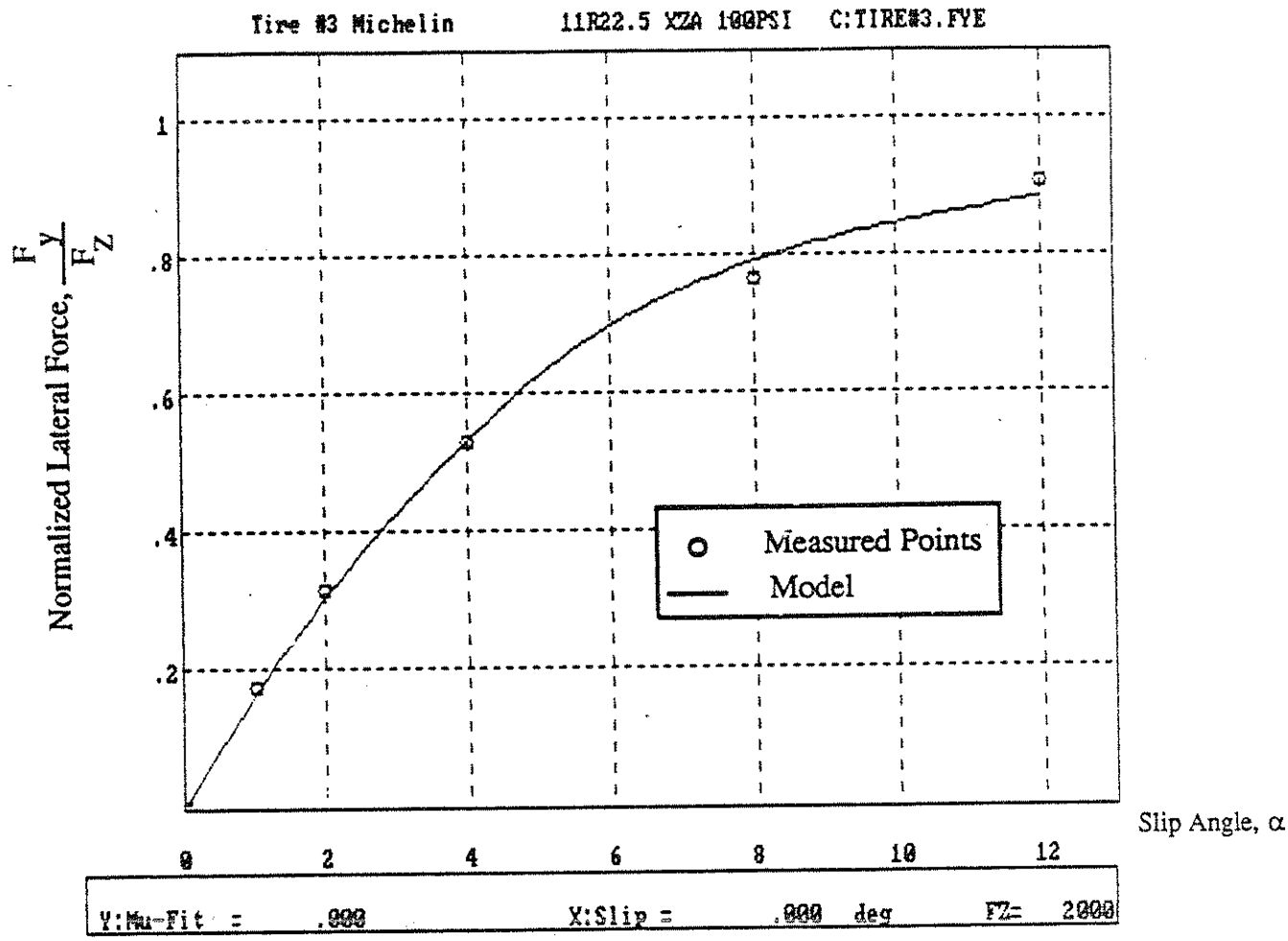

Table of Results

Vertical.Load = 2000.00 lbs

Calfa = 352.99 Lb/deg

Mu = .8840

a/l = .2897

Slip Ang. (deg)	Fy (exp.) lb.	Fy (fitted) lb.	%CH
1.00	347.00	326.21	-5.9906
2.00	626.00	606.54	-3.1089
4.00	1061.00	1063.97	.2800
8.00	1532.00	1583.60	3.3679
12.00	1813.00	1767.97	-2.4835

X^2 = 5509.2070

Figure 7. Results for Tire #3 at 2000 lbs

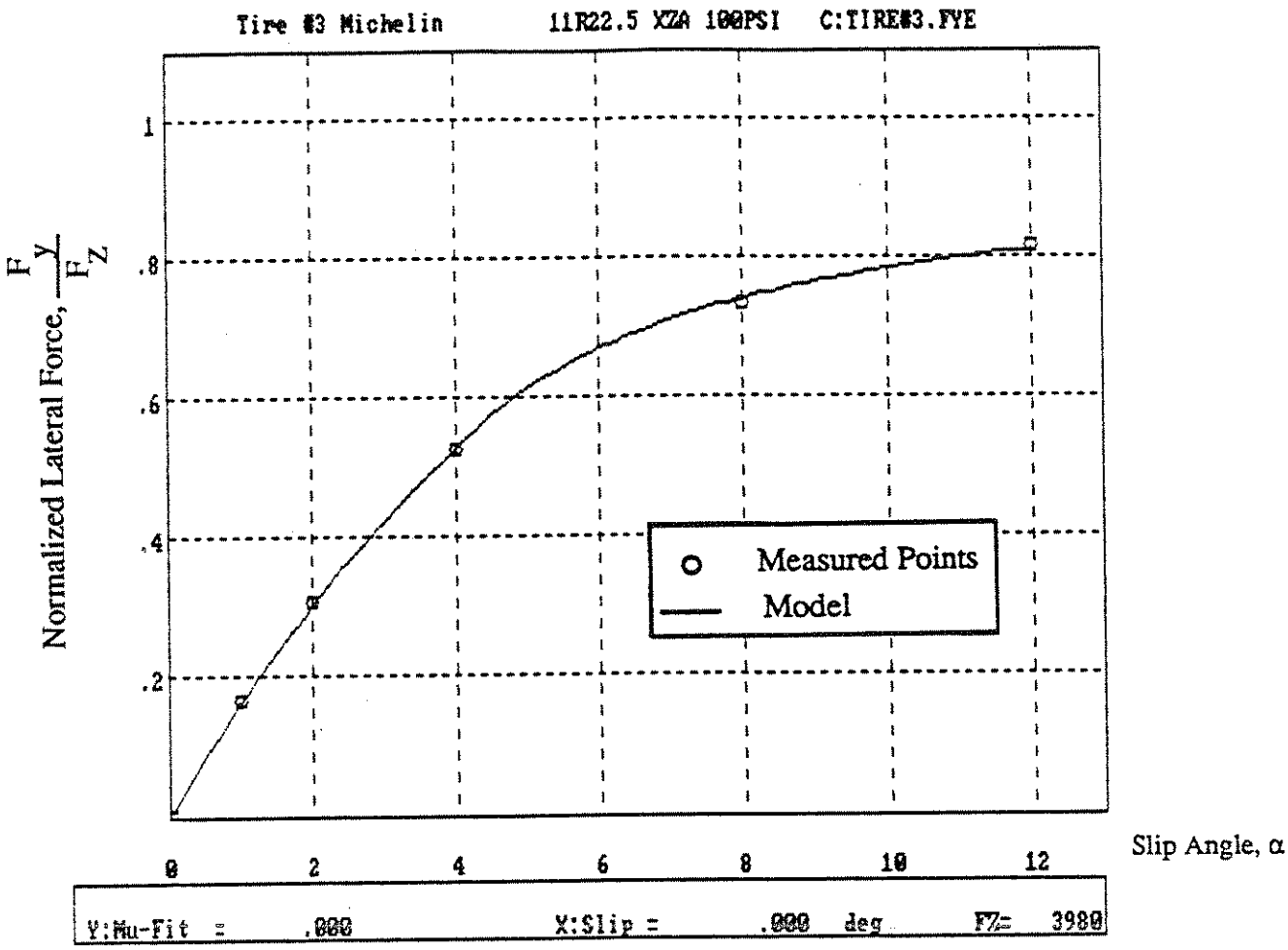

Table of Results
Vertical Load = 3980.00 lbs
Calfa = 700.50 Lb/deg
Mu = .8110
a/l = .2613

Slip Ang. (deg)	Fy (exp.) lb.	Fy (fitted) lb.	%CH
1.00	657.00	646.39	-1.6144
2.00	1223.00	1200.32	-1.8545
4.00	2088.00	2101.16	.6305
8.00	2930.00	2952.34	.7625
12.00	3254.00	3227.62	-.8108

X^2 = 1995.3300

Figure 8. Results for Tire #3 at 3980 lbs

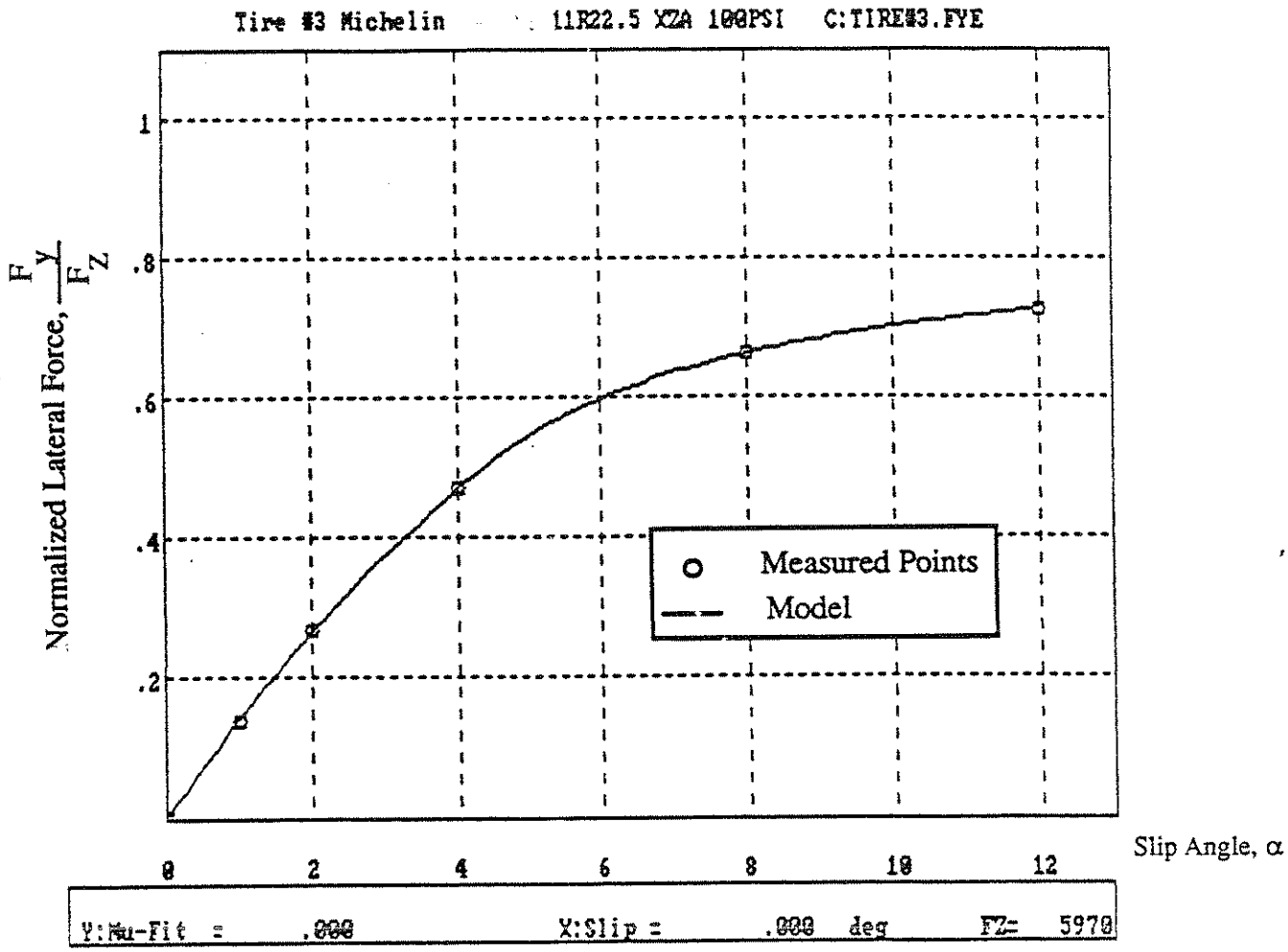

Table of Results
Vertical Load = 5970.00 lbs
Calfa = 908.10 Lb/deg
Mu = .7417
a/l = .2351

Slip Ang. (deg)	Fy (exp.) lb.	Fy (fitted) lb.	%CH
1.00	831.00	845.79	1.7794
2.00	1596.00	1583.26	-.7980
4.00	2805.00	2808.38	.1206
8.00	3965.00	3962.61	-.0602
12.00	4349.00	4350.75	.0403

X^2 = 401.0690

Figure 9. Results for Tire #3 at 5970 lbs

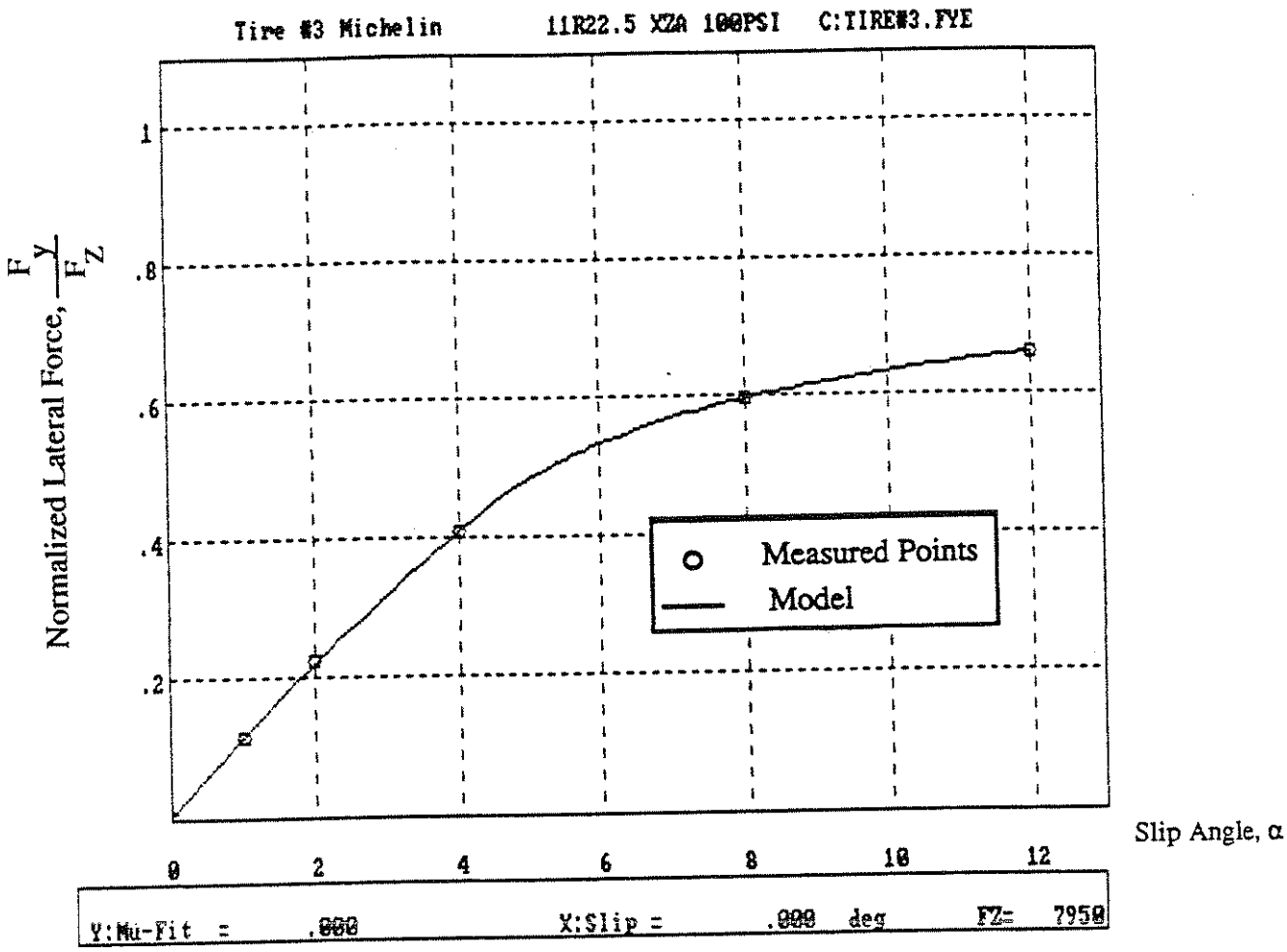

Table of Results
Vertical Load = 7950.00 lbs
Calfa = 962.21 Lb/deg
Mu = .7135
a/l = .1650

Slip Ang. (deg)	Fy (exp.) lb.	Fy (fitted) lb.	%CH
1.00	910.00	919.30	1.0223
2.00	1769.00	1760.49	-.4813
4.00	3240.00	3246.87	.2119
8.00	4761.00	4743.87	-.3597
12.00	5236.00	5248.46	.2380

X^2 = 654.7872

Figure 10. Results for Tire #3 at 7950 lbs

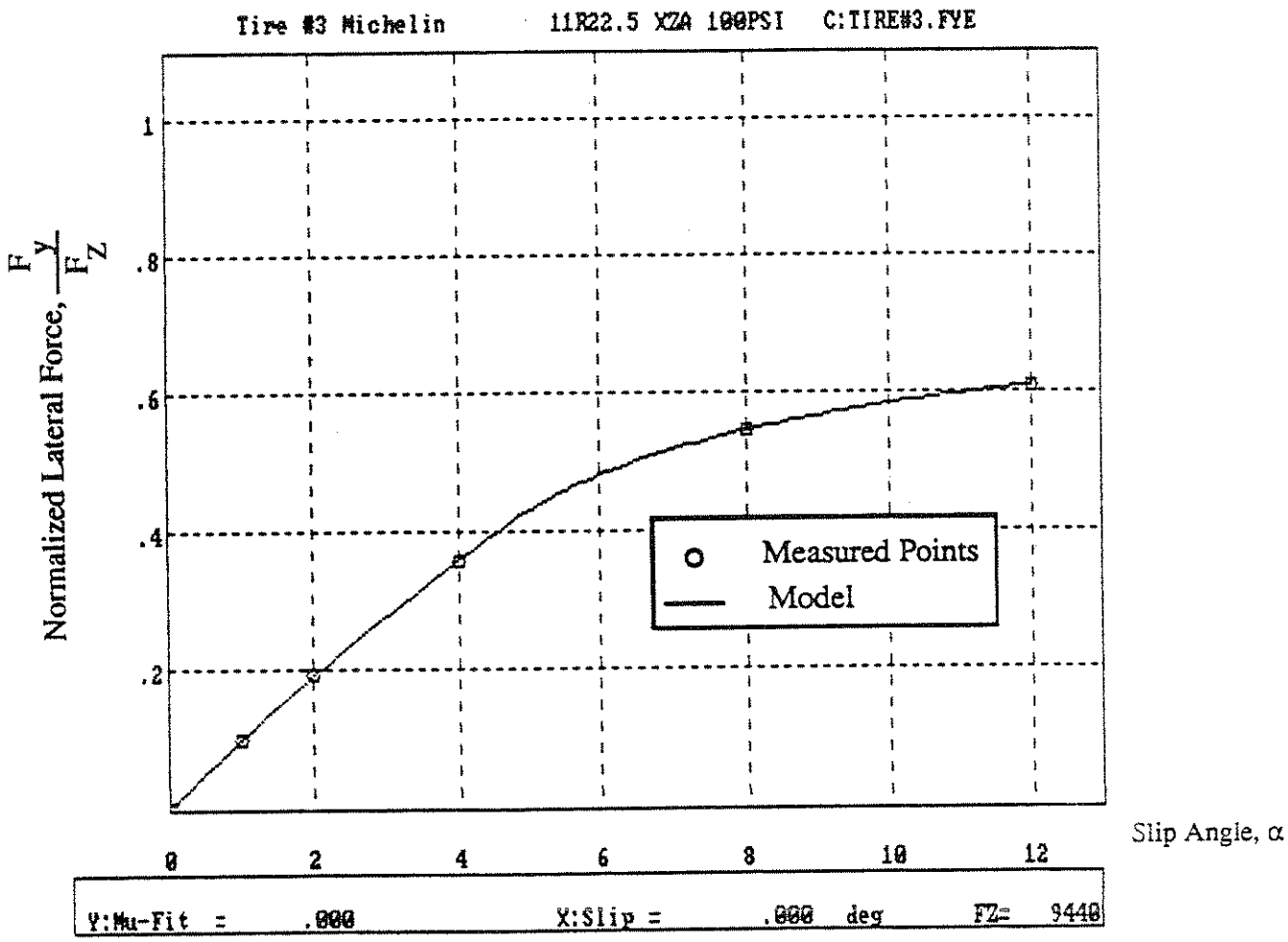

Table of Results
Vertical Load = 9440.00 lbs
Calfa = 970.29 Lb/deg
Mu = .6792
a/l = .1421

Slip Ang. (deg)	Fy (exp.) lb.	Fy (fitted) lb.	%CH
1.00	929.00	935.84	.7366
2.00	1814.00	1807.89	-.3367
4.00	3384.00	3386.84	.0838
8.00	5160.00	5155.55	-.0862
12.00	5758.00	5761.12	.0541

X^2 = 121.6547

Figure 11. Results for Tire #3 at 9440 lbs

TIRE # 6, MICHELIN 11R22.5, 1/3 TREAD.

This tire is the same type as tire # 3 except that 2/3 of the tread groove depth has been worn away, leaving only 1/3 of the original groove depth.

The results of the fitting process for this tire are presented in Figures 12 through 16.

As before, a better fit is obtained at the higher values of normal load — in this case for the center part the curve. The standard error decreases considerably at high loads.

The average overall error for this tire is approximately 1.32%.

In general, we can say that the errors and discrepancies for these fittings are mainly due to the pre-averaging process applied to the experimental data and the uncertainties related to the measuring device. These errors can be greatly reduced if all of the experimental data were used, without pre-averaging, to find the parameters for the tire model. In that case, the data processing program would have more data to work with and it could calculate the uncertainty associated with the experiment for each data point, thereby providing a means for minimizing the standard fitting error.

Influences of Variations in Tire Parameters

Variations from the best fitted parameters for tire # 3 were done to observe the influences of the parameters used in the tire model. Variations in C_α, μ_y and a/L were done for a normal load of 5970.00 lbs, which is close to the nominal one of 6040 lbs. (See Figure 9 showing the experimental and fitted results at 5970 lbs.)

Variations in C_α

C_α was changed by ± 10% from the best fitted value of 908.10 lb/deg. The resulting plots are presented in Figure 17. This parameter primarily influences the initial slope of the curve such that offsets are quite noticeable for slip angles above 2°. A positive increment to C_α increases the adhesion component of the lateral force. The influences of the variations in C_α start to subside at slip angles greater than 12°.

Variations in μ

μ or μ_y was changed by ± 10% from the best fitted value of 0.7417. The results of these changes are shown in Figure 18. The variations in μ introduced a noticeable change on the upper section of the curve, specially for slip angles greater than 4°. That is because μ determines the magnitude of the contribution to lateral force from the sliding zone of the contact patch. Therefore, increasing the value of μ will increase the force at higher slip angles.

Variations in a/L

Figure 19 shows the effects caused by a ± 10% change in a/L from the fitted value of 0.2351. These particular variations in a/L introduced an almost unnoticeable change in the lateral force curves. However, greater changes, ± 45%, produced more noticeable

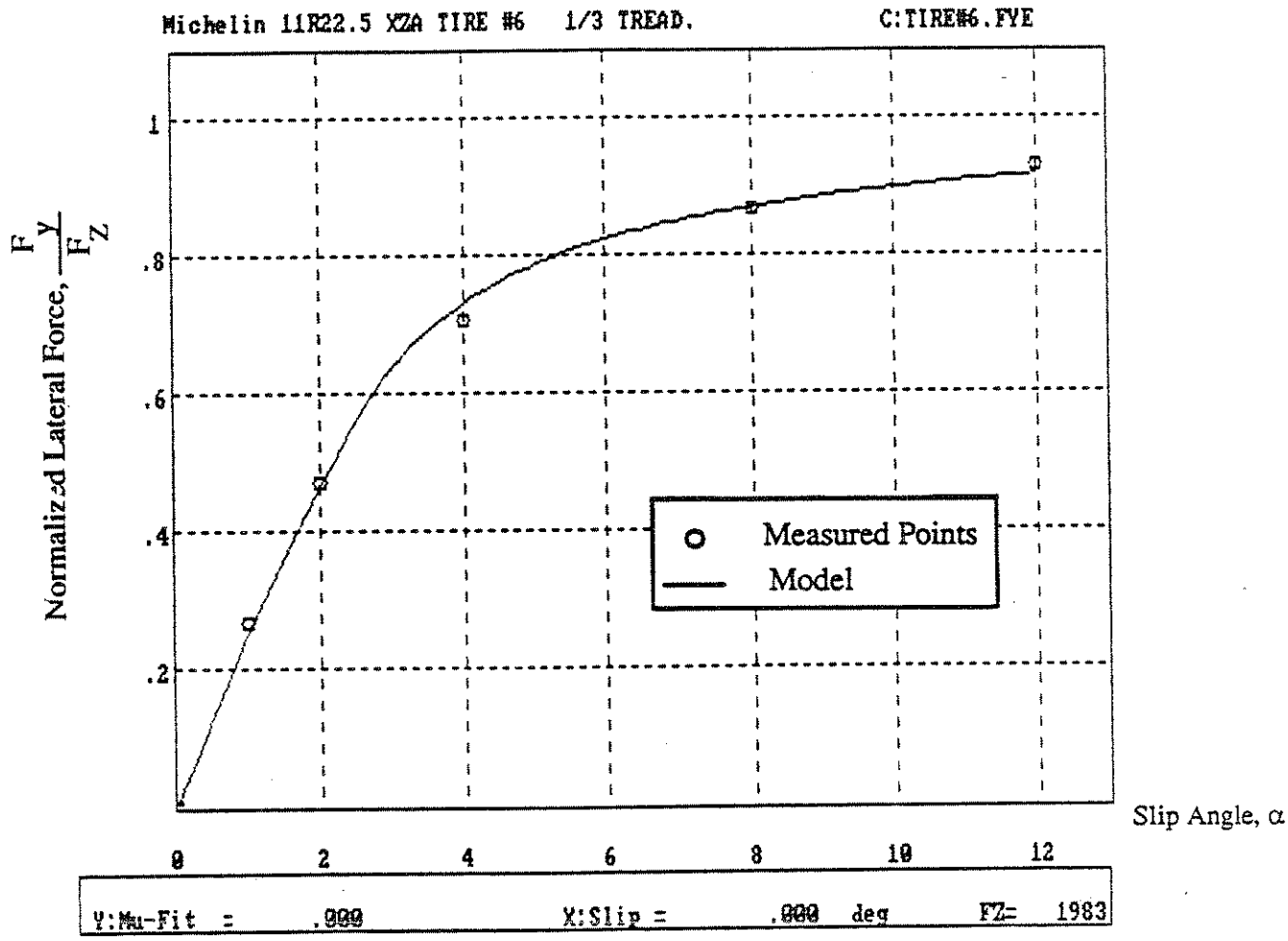

Table of Results
Vertical Load = 1983.65 lbs
Calfa = 539.14 Lb/deg
Mu = .9185
a/l = .1656

Slip Ang. (deg)	Fy (exp.) lb.	Fy (fitted) lb.	%CH
1.00	527.30	498.42	-5.4761
2.00	933.51	927.03	-.6942
4.00	1404.03	1450.91	3.3388
8.00	1725.54	1728.15	.1515
12.00	1846.59	1821.17	-1.3764

X^2 = 3726.1300

Figure 12. Results for Tire #6 at 1983 lbs

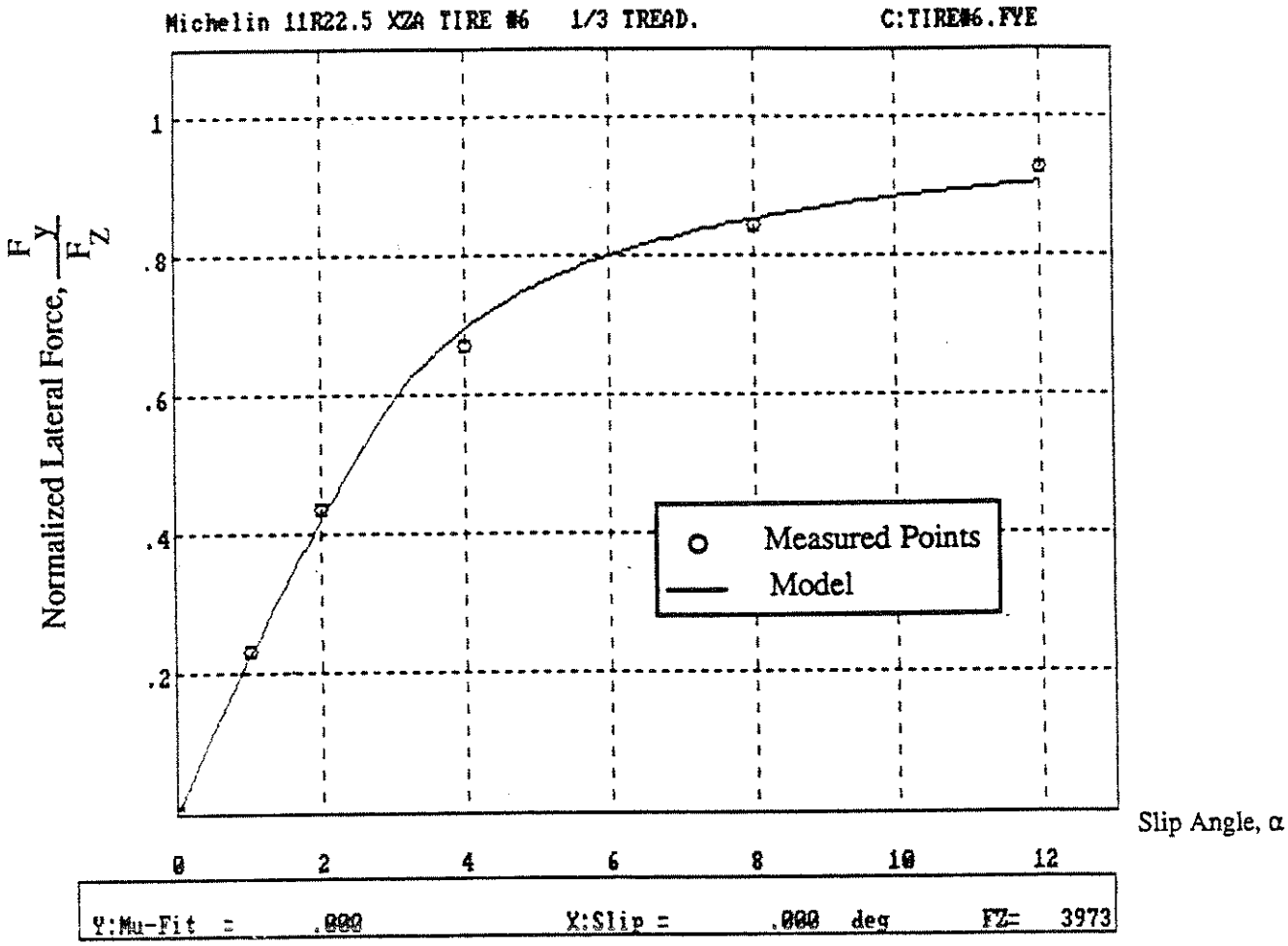

Table of Results
Vertical Load = 3973.84 lbs
Calfa = 975.68 Lb/deg
Mu = .9091
a/l = .1801

Slip Ang. (deg)	Fy (exp.) lb.	Fy (fitted) lb.	%CH
1.00	926.87	903.67	-2.5032
2.00	1731.65	1683.44	-2.7839
4.00	2664.14	2767.80	3.8909
8.00	3348.75	3391.74	1.2838
12.00	3688.28	3601.08	-2.3642

X^2 = 23059.2600

Figure 13. Results for Tire #6 at 3973 lbs

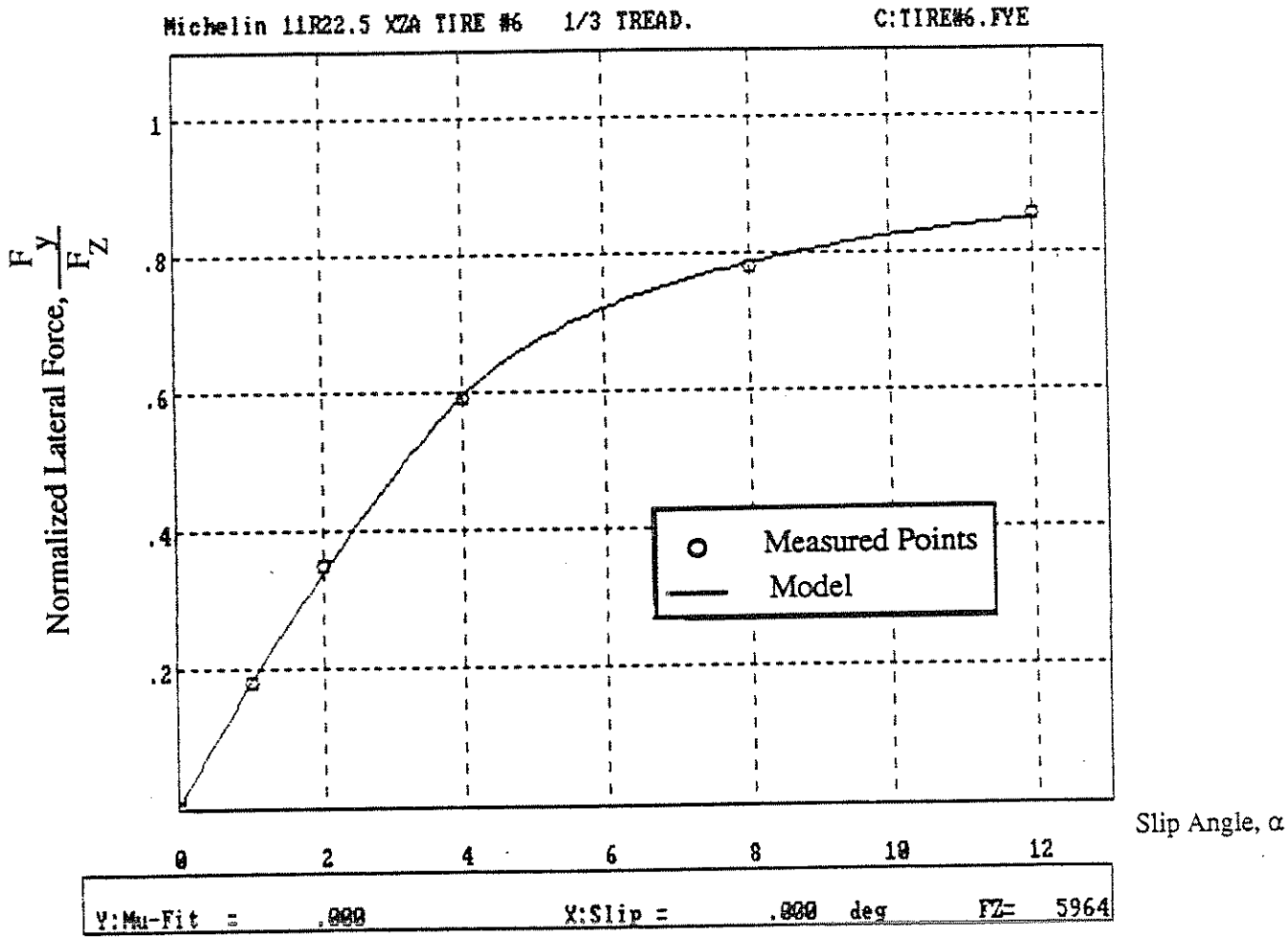

Table of Results
Vertical Load = 5964.34 lbs
Calfa = 1184.22 Lb/deg
Mu = .8529
a/l = .2254

Slip Ang. (deg)	Fy (exp.) lb.	Fy (fitted) lb.	%CH
1.00	1069.82	1095.26	2.3782
2.00	2084.19	2037.86	-2.2230
4.00	3537.56	3554.42	.4766
8.00	4672.24	4696.26	.5141
12.00	5100.59	5079.36	-.4162

X^2 = 4105.8860

Figure 14. Results for Tire #6 at 5964 lbs

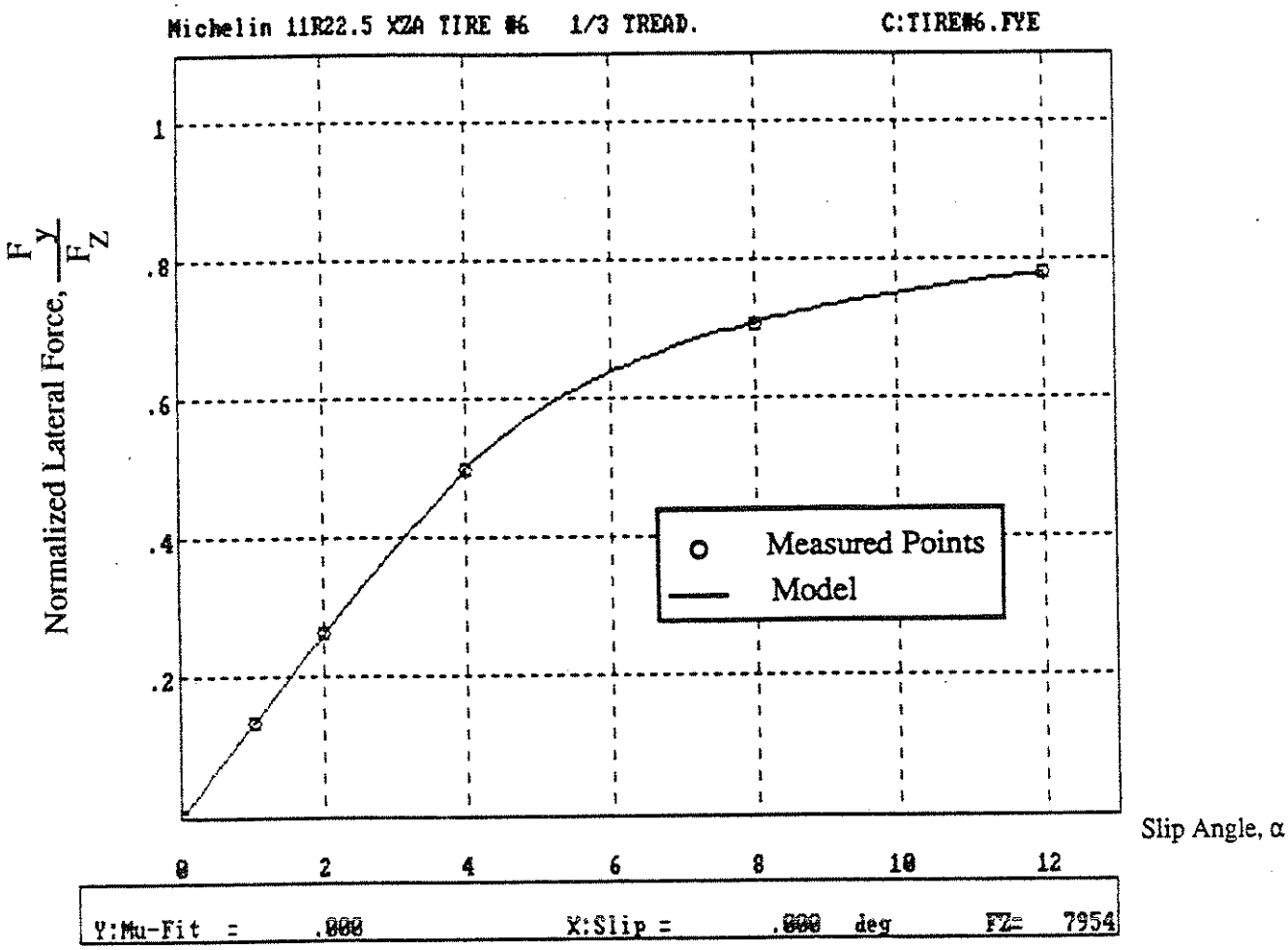

Table of Results
Vertical Load = 7954.22 lbs
Calfa = 1107.89 Lb/deg
Mu = .8695
a/l = .1044

Slip Ang. (deg)	Fy (exp.) lb.	Fy (fitted) lb.	%CH
1.00	1067.42	1075.75	.7804
2.00	2098.03	2091.29	-.3214
4.00	3964.40	3960.40	-.1010
8.00	5626.41	5647.88	.3816
12.00	6230.18	6214.05	-.2590

X^2 = 852.1083

Figure 15. Results for Tire #6 at 7954 lbs

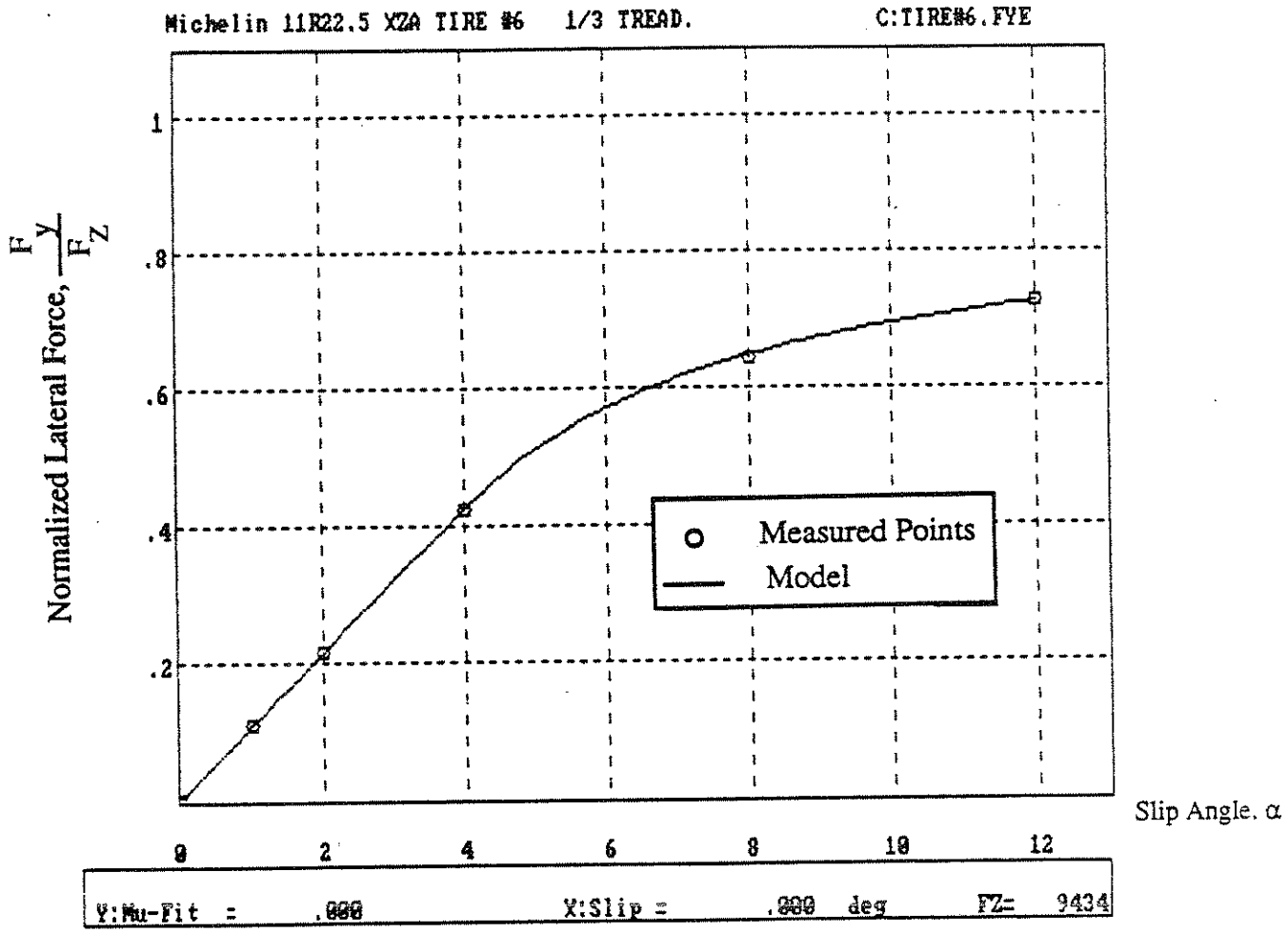

Table of Results
Vertical Load = 9434.79 lbs
Calfa = 1045.86 Lb/deg
Mu = .8525
a/l = .0507

Slip Ang. (deg)	Fy (exp.) lb.	Fy (fitted) lb.	%CH
1.00	1032.45	1033.01	.0542
2.00	2039.29	2041.39	.1032
4.00	4001.54	3990.05	-.2872
8.00	6091.67	6126.67	.5746
12.00	6873.95	6848.62	-.3685

X^2 = 2003.3690

Figure 16. Results for Tire #6 at 9434 lbs

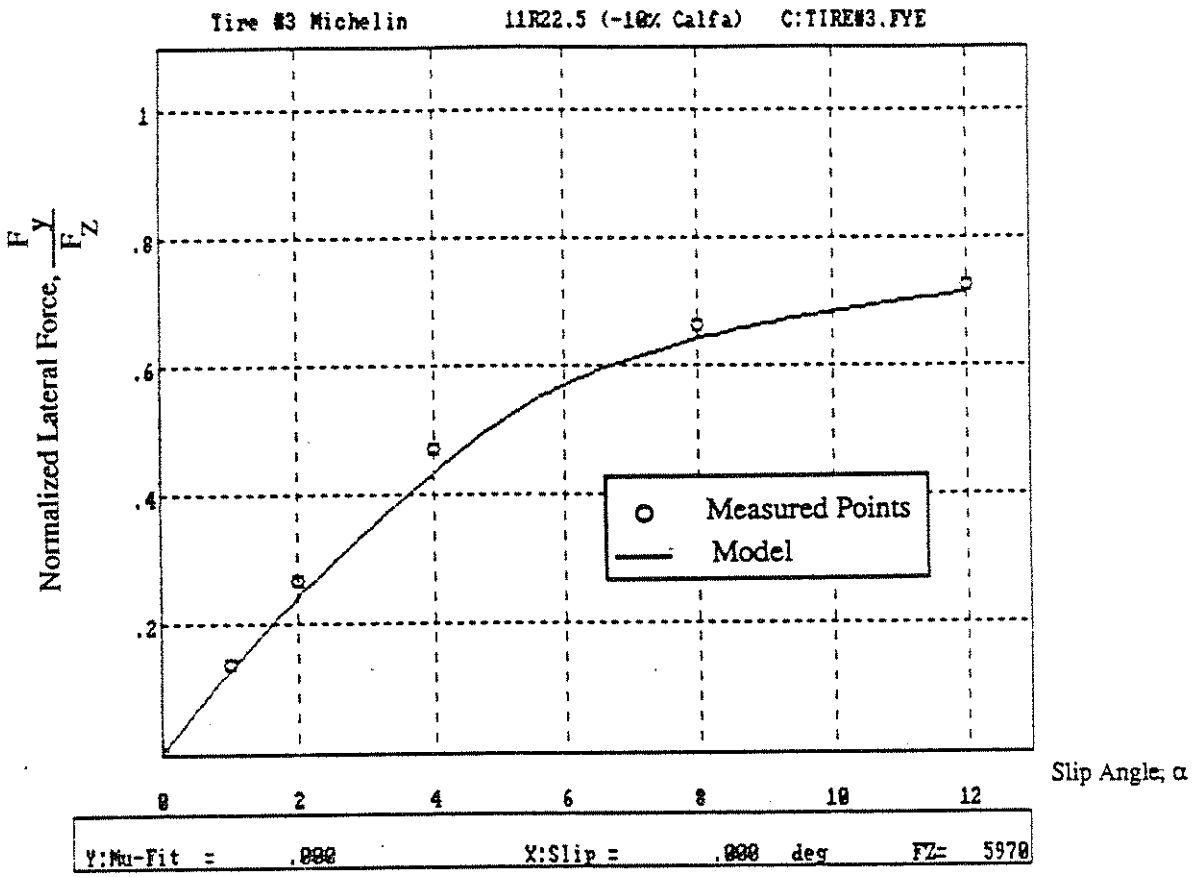

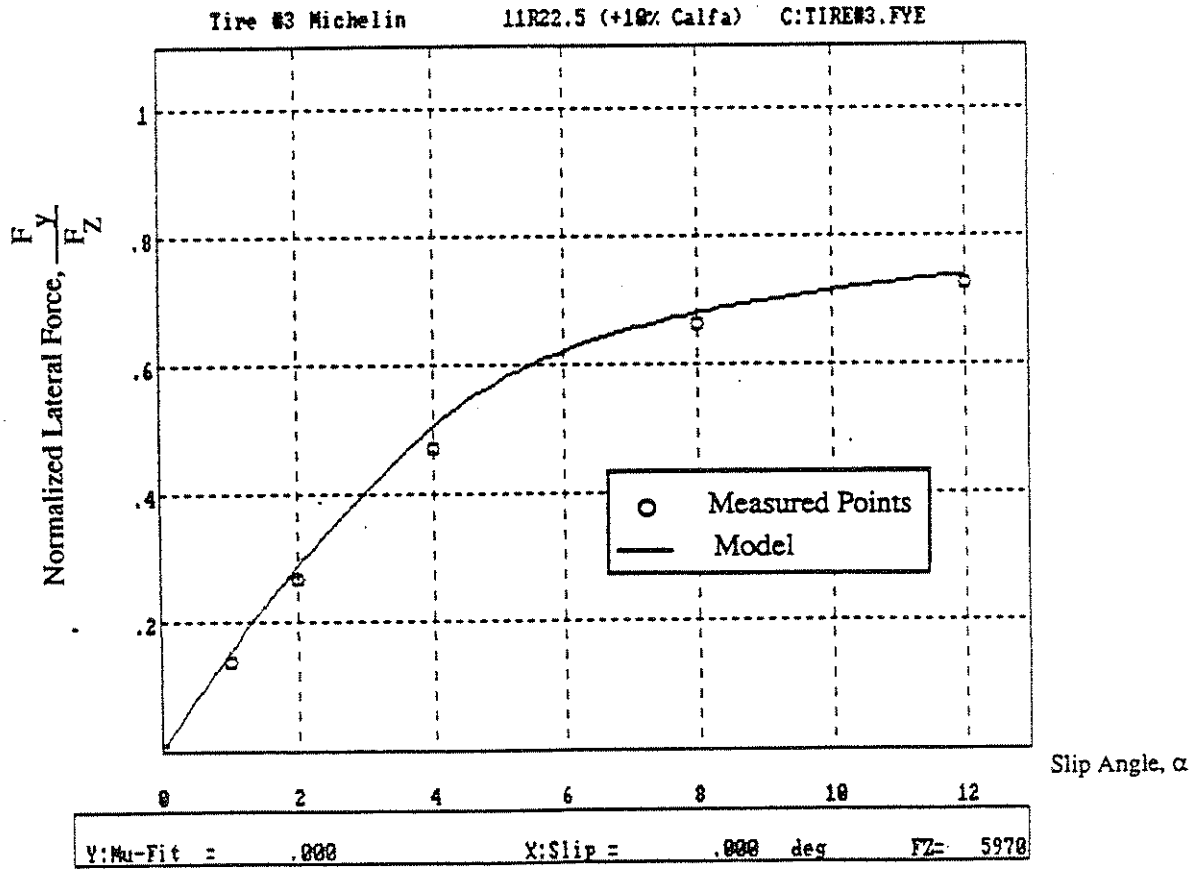

Figure 17. Variations of ±10% in C_α at 5970 lb

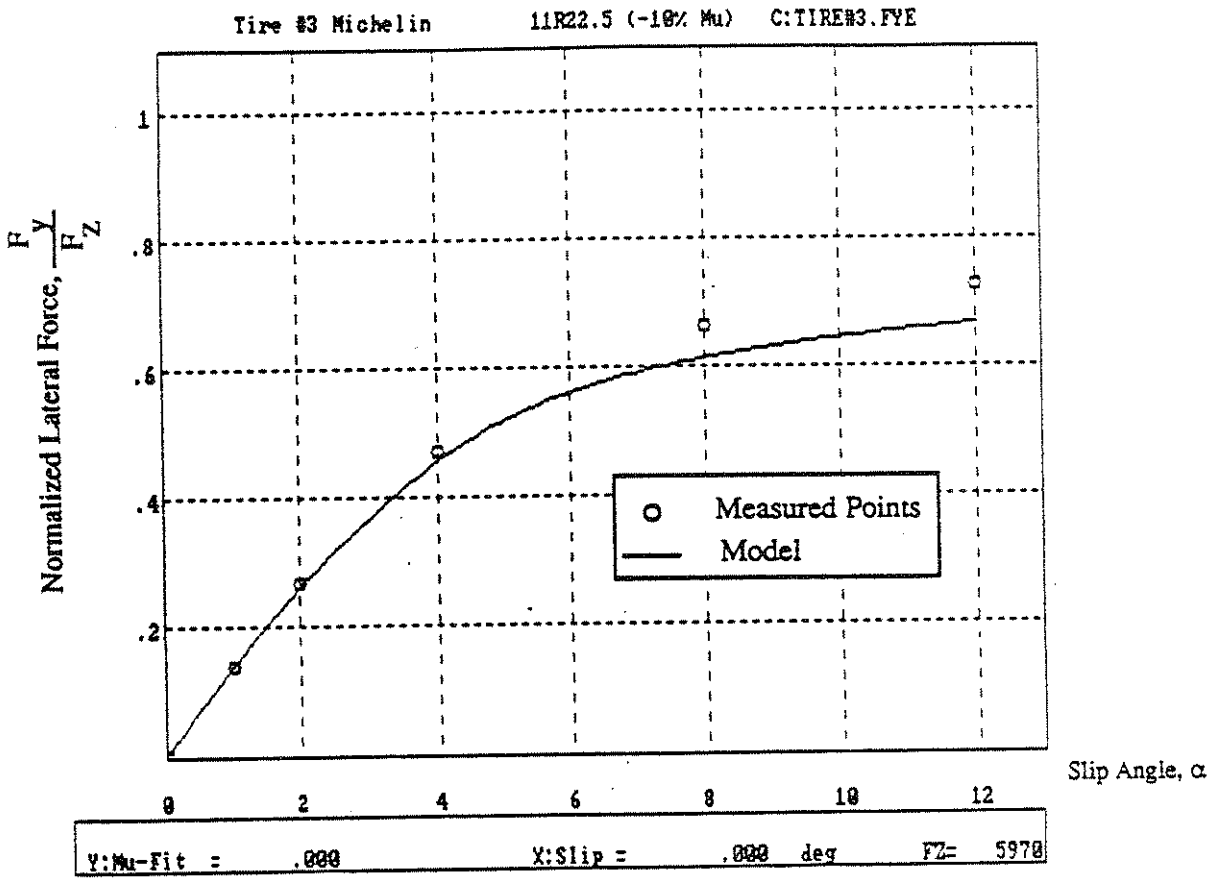

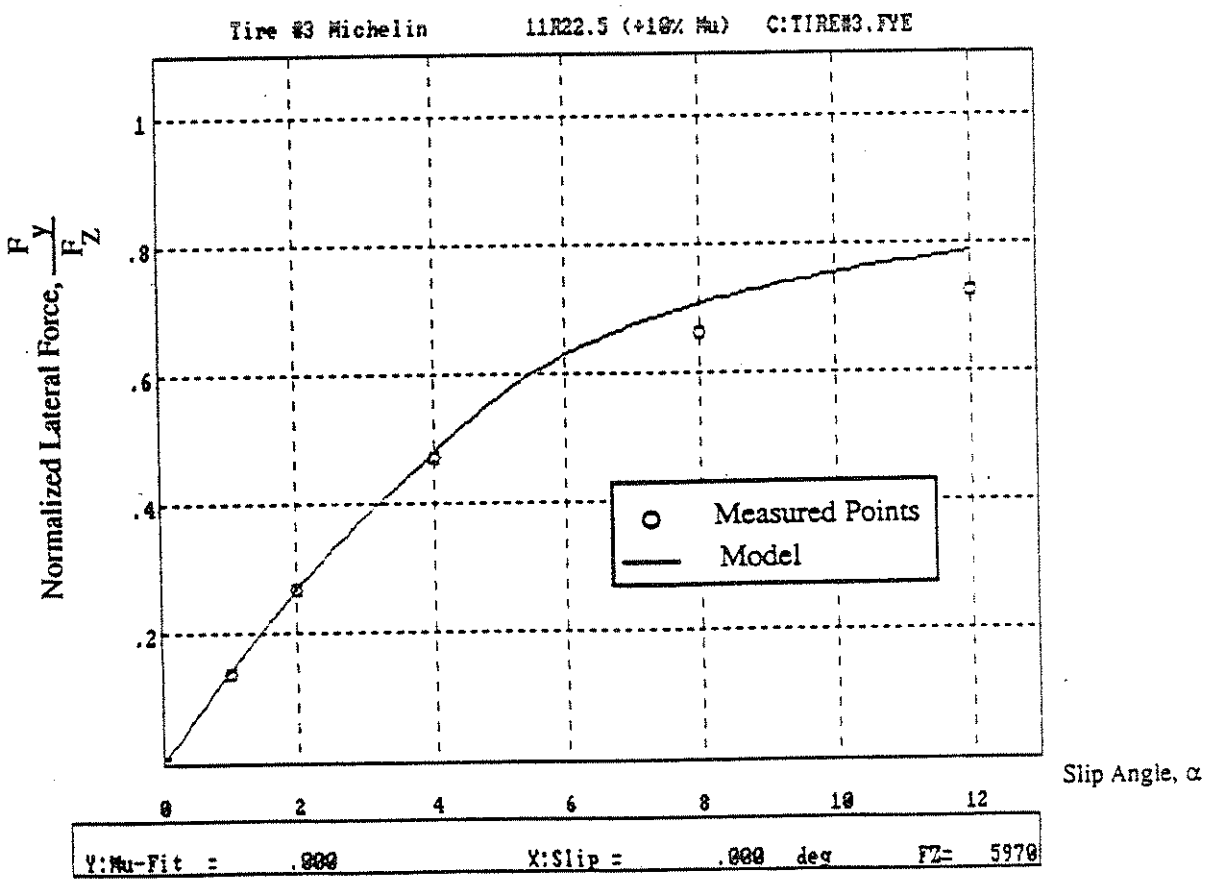

Figure 18. Variations of ±10% in μ_y at 5970 lb

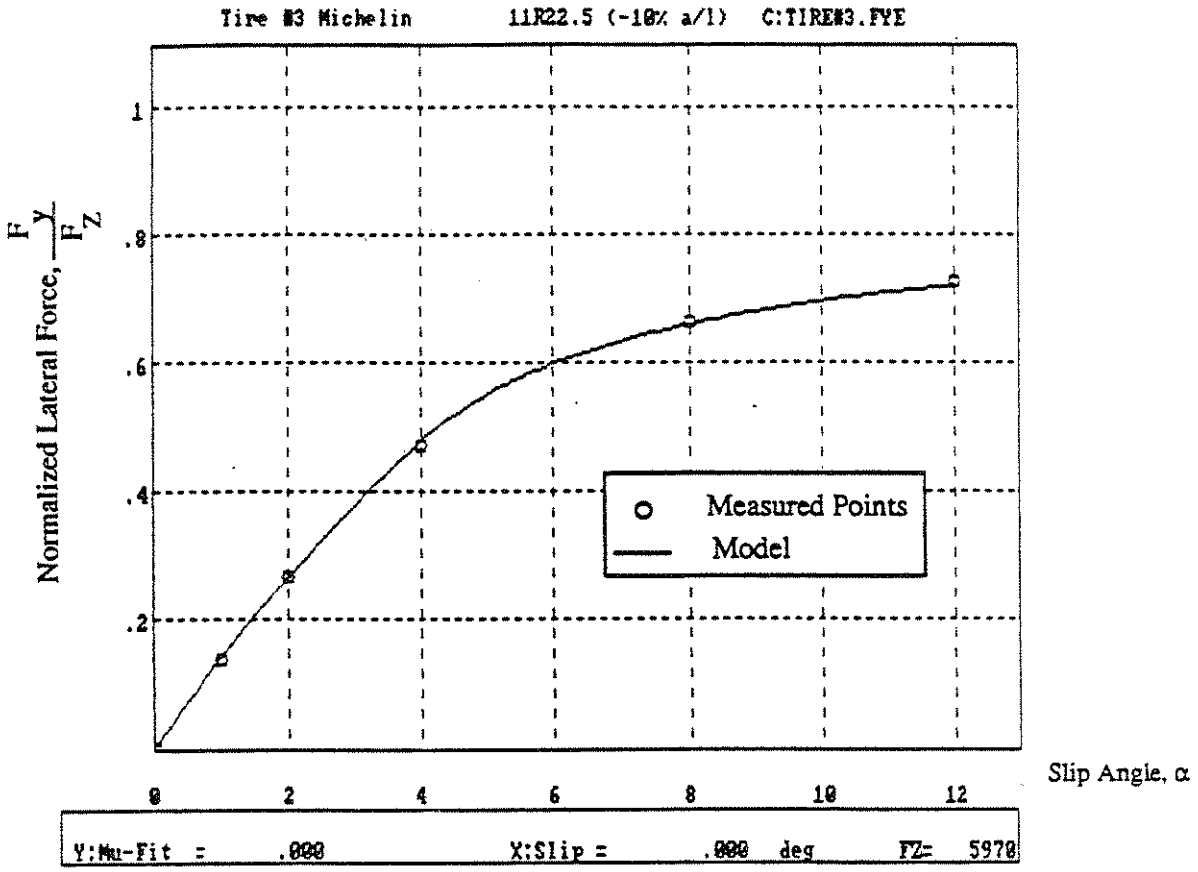

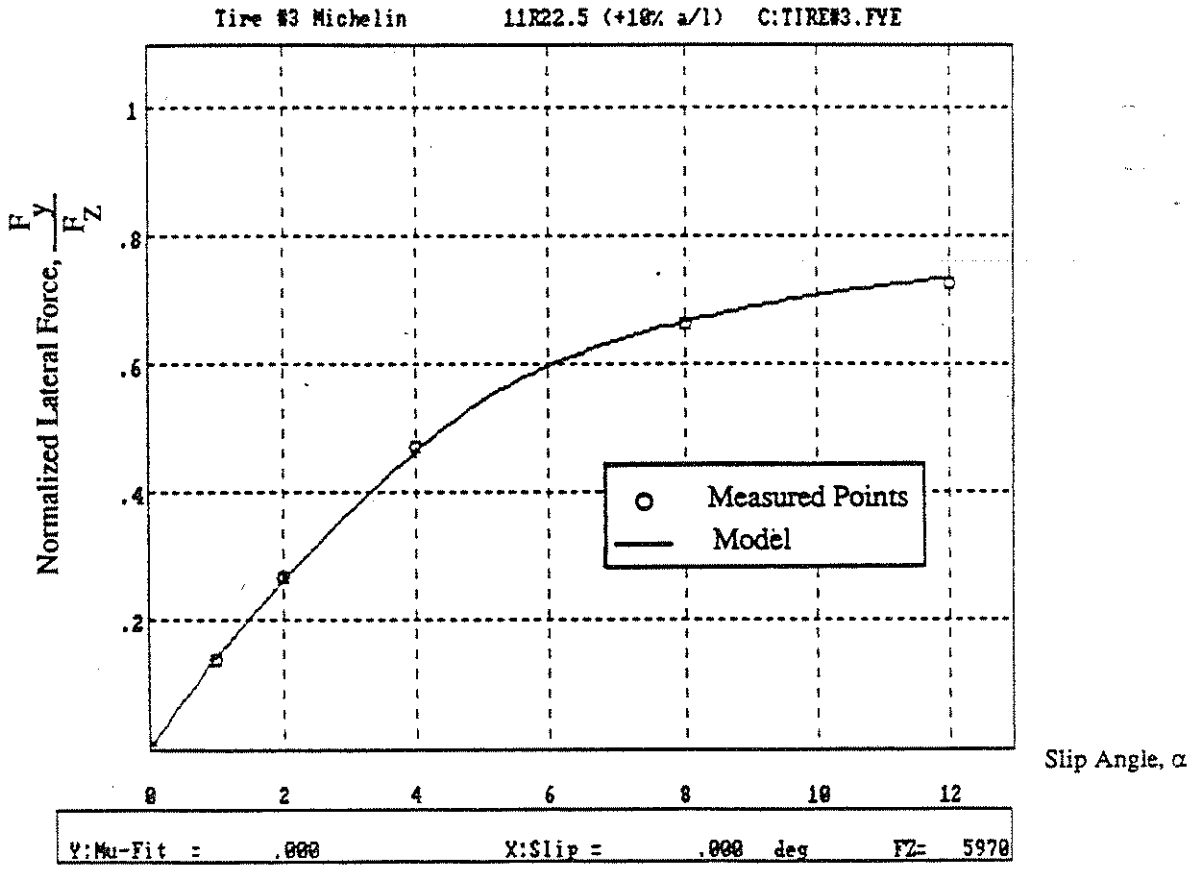

Figure 19. Variations of ±10% in a/L at 5970 lb

changes in the curves (see Figure 20). These deviations are substantial at slip angles of 4°. At 4°, a 45% increase in a/L causes a decrease in lateral force compared to the point produced at the fitted value of a/L. However, at larger slip angles the increase in a/L produces an increase in lateral force. A 45% decrease in a/L produces just the opposite effects, as illustrated at the top of Figure 20.

As the shape parameter, a, becomes larger, the pressure distribution becomes smaller on the ends and higher in the middle. When the shape parameter, a, is larger, the sliding boundary will be located more towards the front of the contact patch than it would have been if a/L were not increased and everything else remained the same. This, in effect, makes C_α, less effective in determining lateral force as slip angle increases and it makes μ_y more effective at large slip angles in the range from 8 to 12 degrees. In other words, the shape of the pressure distribution as represented by a/L can have a rather complicated influence on the shape of the lateral force curves at slip angles above 4 degrees. Nevertheless, at 4 degrees and less, increasing a/L reduces the lateral force predicted by the tire model.

Representation of Fitted Values

All fitted parameters, C_α, μ_y and a/L , for all six test tires, have been represented as a function of load, F_Z, and velocity, V. The general parametric equation used for this purpose is of the form:

$$C = C_0 + C_1 * (F_Z - F_{Z0}) + C_2 * (F_Z - F_{Z0})^2 + C_3 * (V - V_0) + C_4 * (V - V_0)^2$$

where the constants C_3 and C_4 are set equal to zero for this study, since the tests were performed at a single low speed and values of C_3 and C_4 are not needed in fitting the data. By using a statistical polynomial regression fit, constants C_1 and C_2 were found for each of the quantities, C_α, μ_y and a/L . Figures 21, 22, and 23 show the results of the regression for all six tires.

Figure 21 shows that the worn tires, 6 and 5, exhibit greater cornering stiffnesses than the other tires. Peak values are also reached at lower loads for the worn tires. The fully treaded tires exhibit similar characteristics, but they have their peak values in the neighborhood of 8,000 lbs.

Interestingly, for the new tires these results for cornering stiffness indicate that both the low profile 11:22.5 and the normal profile 11:22.5 have nearly the same cornering stiffnesses at all loads and that both samples of each type of tire are nearly identical.

Figure 22 shows that the 2/3 worn tire has a greater value of μ for all values of vertical load. Tire #5, 1/2 worn, has greater μ than the rest of the new tires for normal forces greater than 4,000 lbs. (This is the only tire data yielding a negative value of curvature.) Since the flatbed machine only operates at low speed and its surface is not a real road, the friction values may not be representative of those obtained in service as some types of roads. However, results from the flatbed have been found to be similar to those obtained from testing tires on good, dry concrete surfaces.

Again the new tires look to be remarkably similar.

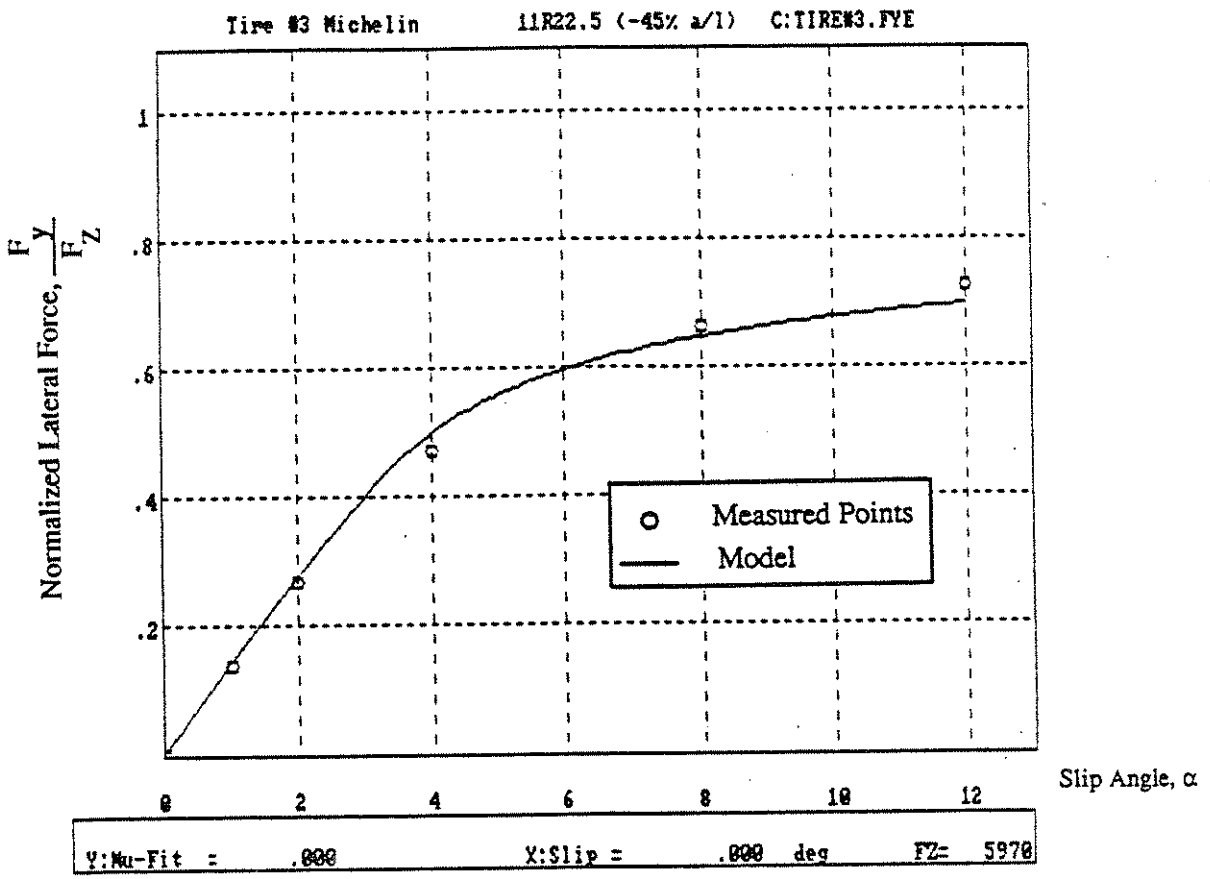

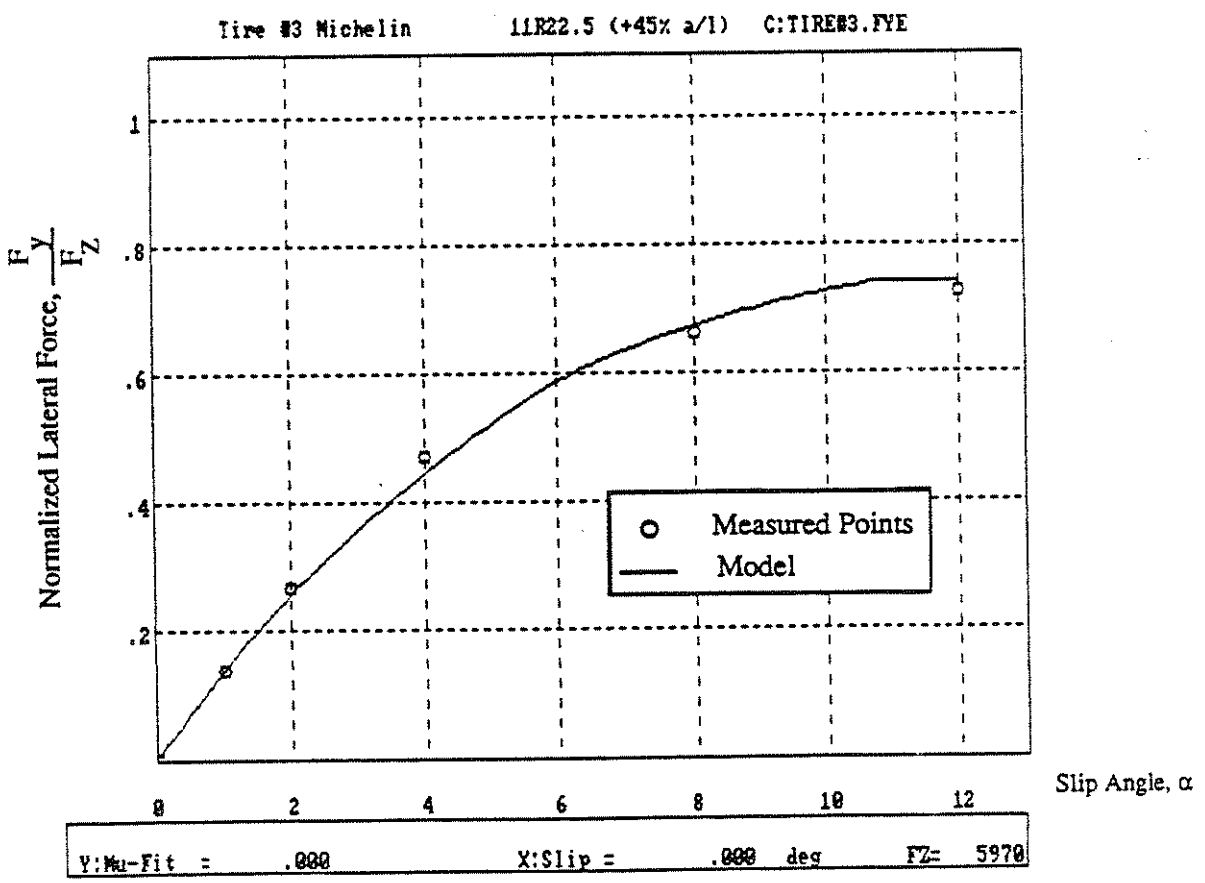

Figure 20. Variations of ±45% in a/L at 5970 lb

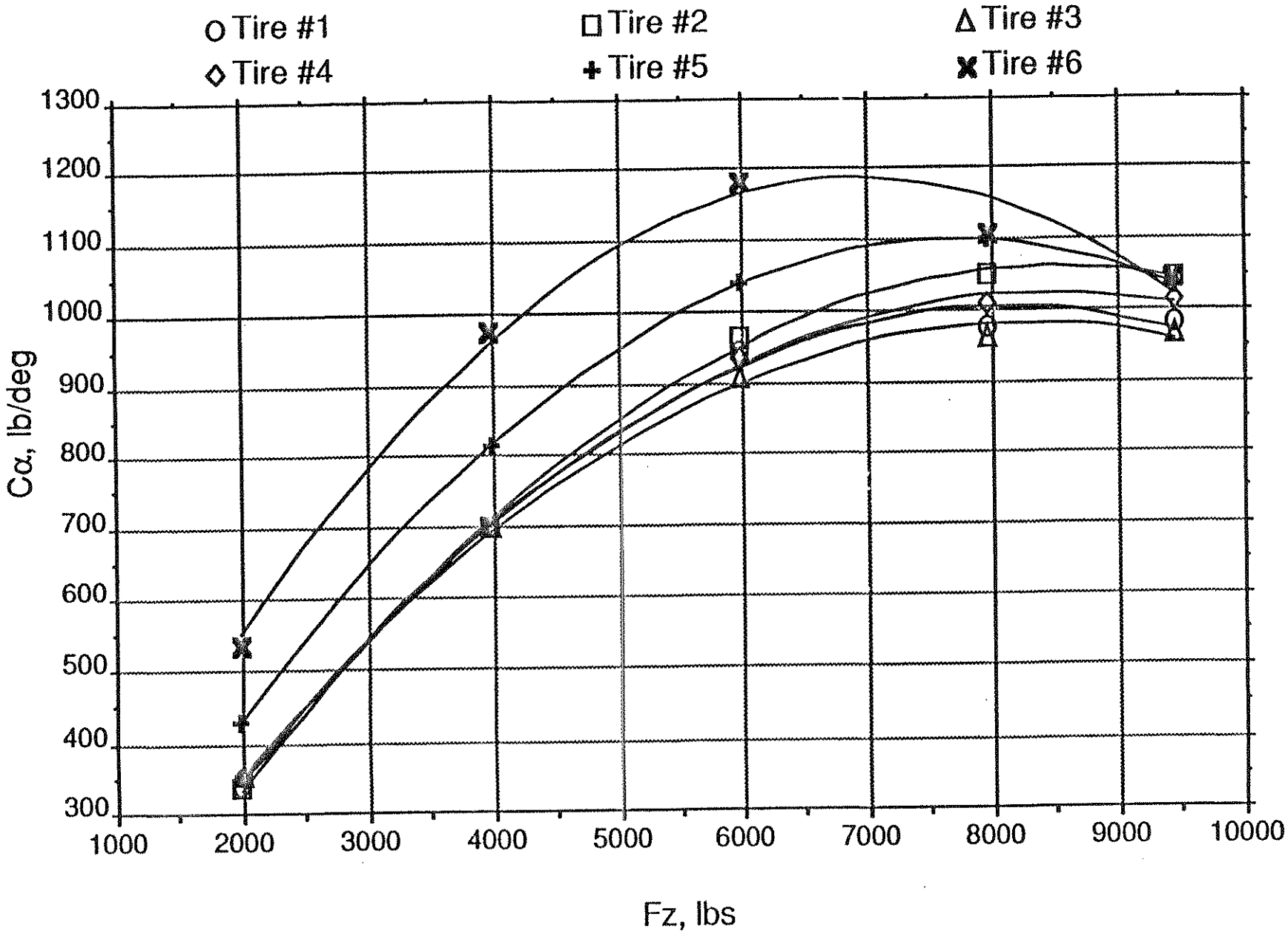

Figure 21. Cornering Stiffness, Cα

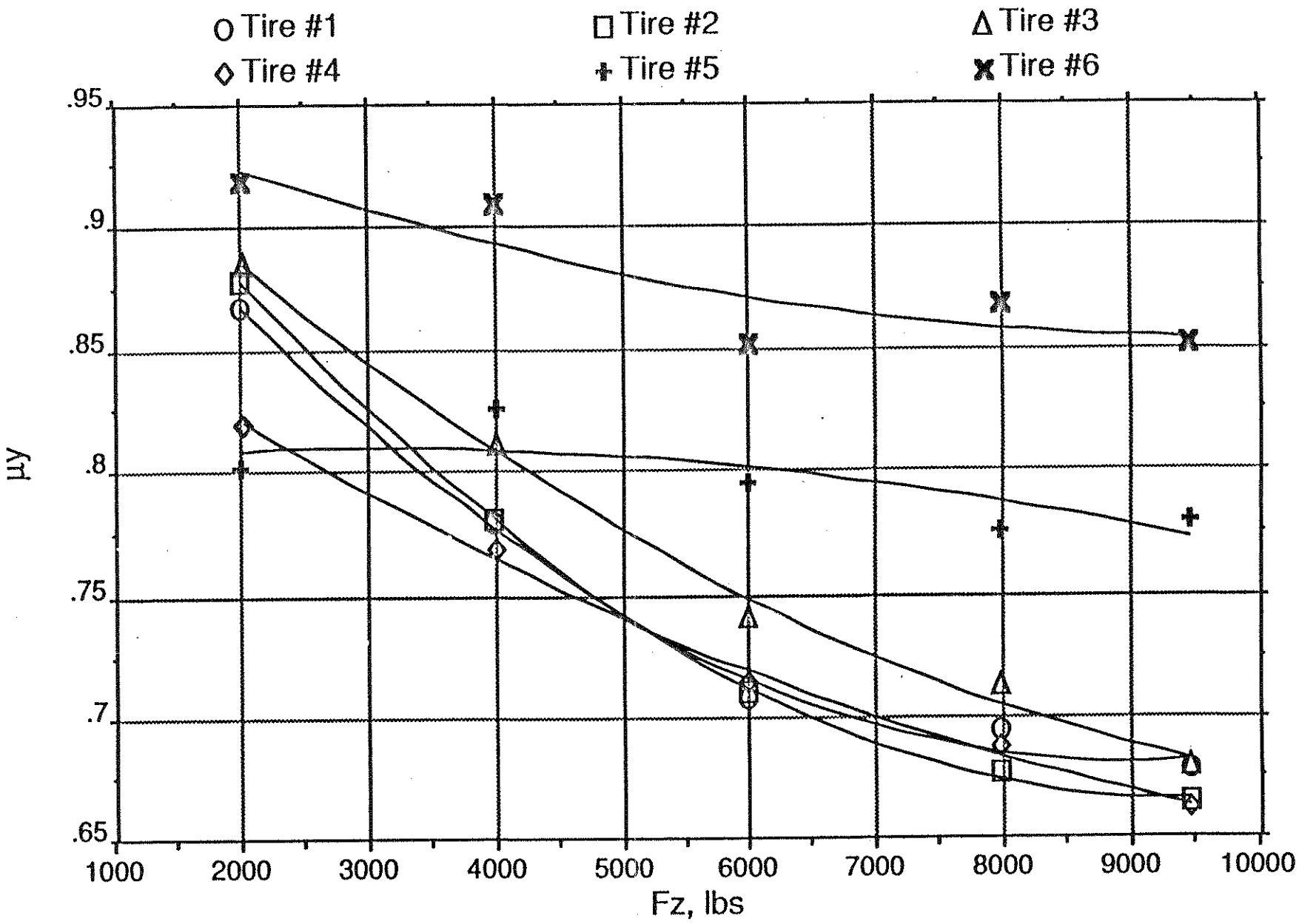

Figure 22. Lateral Frictional Coupling, μy

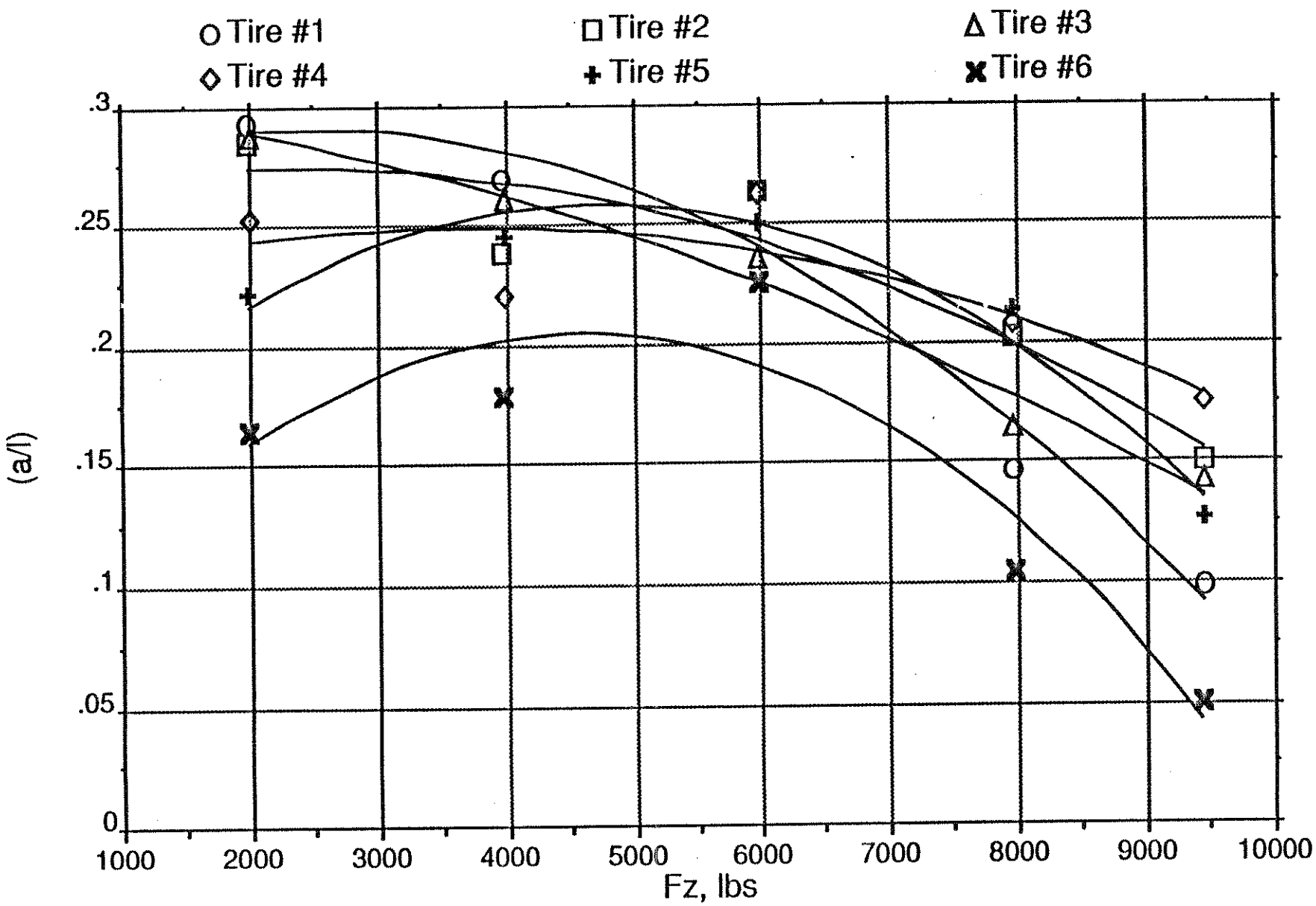

Figure 23. Pressure Distribution Parameter, a/l

Figure 23 depicts the behavior of a/Lwith respect to vertical load. In this case tire #6 exhibits the lowest values of all the tires. All tires present a negative curvature. The peak values of a/L come at heavier loads for the worn tires (that is, in between 4,500 lbs and 5,500 lbs for the worn tires, while the new tires have their maximum values in the neighborhood of 3,000 lbs).

An example data set for this representation is given below for tire #1.

$$C_\alpha = 929.37 + 0.0725 * (F_Z - F_{Z0}) - 1.776E\text{-}05 * (F_Z - F_{Z0})^2$$

$$\mu_y = 0.7139 - 2.2479E\text{-}05 * (F_Z - F_{Z0}) + 3.846E\text{-}09 * (F_Z - F_{Z0})^2$$

$$a/L = 0.2382 - 2.9422E\text{-}05 * (F_Z - F_{Z0}) - 4.082E\text{-}09 * (F_Z - F_{Z0})^2$$

where F_{Z0} is the nominal load and has a value of 6,040 lbs.

It is important to point out that this regression will induce another uncertainty to the fitted values. This uncertainty is the smallest for C_α which is more precisely defined through a better fit. The parametric values, such as those listed above for tire #1, may be used to study tire behavior in predictive computer programs such as the one described in the next section.

4.0 PREDICTION OF TRACTION FIELDS

The enhanced representation of side force capability has been incorporated into a model for predicting traction fields under conditions of combined longitudinal and lateral slip. (This model has been programmed for use on IBM PC's. Persons interested in computerized versions of the models should contact the authors of this report.) This section provides an overview of the elements of the methodology for predicting traction fields.

A Brief Description of the Computer Program

The computerized model predicts the tire forces, F_X and F_Y, the aligning torque, and roll-off tables relating F_X and F_Y for slip angles varying from 0° to 20° (0.35 radians) and longitudinal slips varying from 0.0 to 1.0 (free rolling to locked wheel). The equations described in appendix A are used in the computerized model for predicting traction fields. English units are used throughout the program.

The computer program is capable of generating tables and plots in the above ranges, as well as computing a single table of forces and aligning moments for a specified values of either the slip angle α or the longitudinal slip S_x. The calculations are also performed at constant values of load and velocity.

Description of Tire Parameters

Clearly, tire parameters must be supplied to the computer program. As discussed previously, all the tire parameters are represented by functions of the following form:

$$C = C_0 + C_1 * (F_Z - F_{Z0}) + C_2 * (F_Z - F_{Z0})^2 + C_3 * (V - V_0) + C_4 * (V - V_0)^2$$

where:

F_{Z0}	=	tire nominal load, lbs
V_0	=	tire nominal speed, mph.
C	=	the parameter in question
C_0	=	value of the parameter at nominal load and velocity.
C_1	=	rate of change with respect to load
C_2	=	quadratic term or curvature with respect to load.
C_3	=	rate of change with respect to velocity
C_4	=	quadratic term or curvature with respect to velocity.
F_Z	=	simulation load, lbs
V	=	simulation velocity, mph

This equation accounts for the changes in basic tire parameters associated with operating at different speeds and loads.

In addition to the values of the tire parameters at their nominal values the program for evaluating traction fields requires the following coefficients:

- **Cornering Stiffness, C_α**

  Cornering stiffness is obtained from flat bed measurements. The units are entered in Lb/deg. The coefficients with respect to load and velocity are in the following units:

Coefficient	Units
C_1	lb/deg/lb
C_2	lb/deg/lb^2
C_3	lb/deg/mph
C_4	lb/deg/mph^2

- **Lateral frictional coupling, μ_y**

  This parameter is obtained from flat bed measurements, mobile dynamometer measurements, or theoretically derived levels of friction. The parameter is dimensionless. The coefficients with respect to load and velocity are in the following units:

Coefficient	Units
C_1	1/lb
C_2	1/lb^2
C_3	1/mph
C_4	1/mph^2

- **Longitudinal frictional coupling, μ_x**

This parameter is obtained from the tire mobile dynamometer measurements or theoretical considerations. The parameter is dimensionless. The coefficients with respect to load and velocity are in the following units:

Coefficient	Units
C_1	1/lb
C_2	$1/lb^2$
C_3	1/mph
C_4	$1/mph^2$

- **Longitudinal stiffness, C_S**

This parameter is also obtained from the tire mobile dynamometer measurements. The parameter has units of lb/unit slip. The coefficients with respect to load and velocity are in the following units:

Coefficient	Units
C_1	lb/lb
C_2	lb/lb^2
C_3	lb/mph
C_4	lb/mph^2

- **Pressure distribution parameter, a/L**

This parameter is obtained from flat bed measurements, as explained in the previous chapter. This parameter is dimensionless. The coefficients with respect to load and velocity are in the following units:

Coefficient	Units
C_1	1/lb
C_2	$1/lb^2$
C_3	1/mph
C_4	$1/mph^2$

- **Pneumatic trail, X_P**

This parameter is obtained from flat bed measurements usually at a slip angle of 1°. The parameter has units of inches. The coefficients with respect to load and velocity are in the following units:

Coefficient	Units
C_1	in/lb
C_2	in/lb^2
C_3	in/mph
C_4	in/mph^2

- **Lateral deflection stiffness, C_y**

This parameter is obtained from flat bed measurements too. The parameter has units of lb/in. The coefficients with respect to load and velocity are in the following units:

Coefficient	Units
C_1	lb/in/lb
C_2	lb/in/lb^2
C_3	lb/in/mph
C_4	lb/in/mph^2

- **Friction reduction factor, A_S**

This parameter is also obtained from the tire mobile dynamometer measurements and indicates the variation of the total frictional coupling with respect to sliding velocity. The parameter has units of sec/ft. The coefficients with respect to load and velocity are in the following units:

Coefficient	Units
C_1	sec/ft/lb
C_2	sec/ft/lb^2
C_3	sec/ft/mph
C_4	sec/ft/mph^2

Example Predictions

Tire #1, the 11/80 R 22.5 Pilote, has been used to illustrate the types of results predicted by the model. The values used for the lateral properties, C_α, and a/L, are those presented in the previous chapter. C_y and X_P were deduced from flatbed data. The properties, C_S and A_S, were derived from previously existing tire data. The frictional parameters, μ_x and μ_y, are based on flat bed data in this case. The computed results, shown in Figures 24 through 27, are for a load of 6,040 lbs and a velocity of 40 mph. Appendix B contains a numerical listing of the parametric values as they were entered into the computer. It also contains tabulations of the computed results.

The upper most curve in Figure 24 represents the same side force situation as that discussed previously (see Figure 4), except that in this case the friction level is being influenced by sliding velocity through the non-zero value of A_S, the friction reduction factor. Hence, the value of side force starts to decline for slip angles greater than approximately 12 degrees. The other curves in Figure 24 show the influences of increasing amounts of longitudinal slip on lateral force. Clearly, lateral force is greatly reduced, even at large slip angles, if longitudinal slip is above 0.25.

The influences of slip angle on longitudinal force are illustrated in Figures 25 and 26. The presentation in Figure 26 is easier to interpret even though both figures present equivalent information. The upper curve in Figure 26 is a traditional presentation of longitudinal force as a function of longitudinal slip. The other curves in Figure 26 show that longitudinal force is

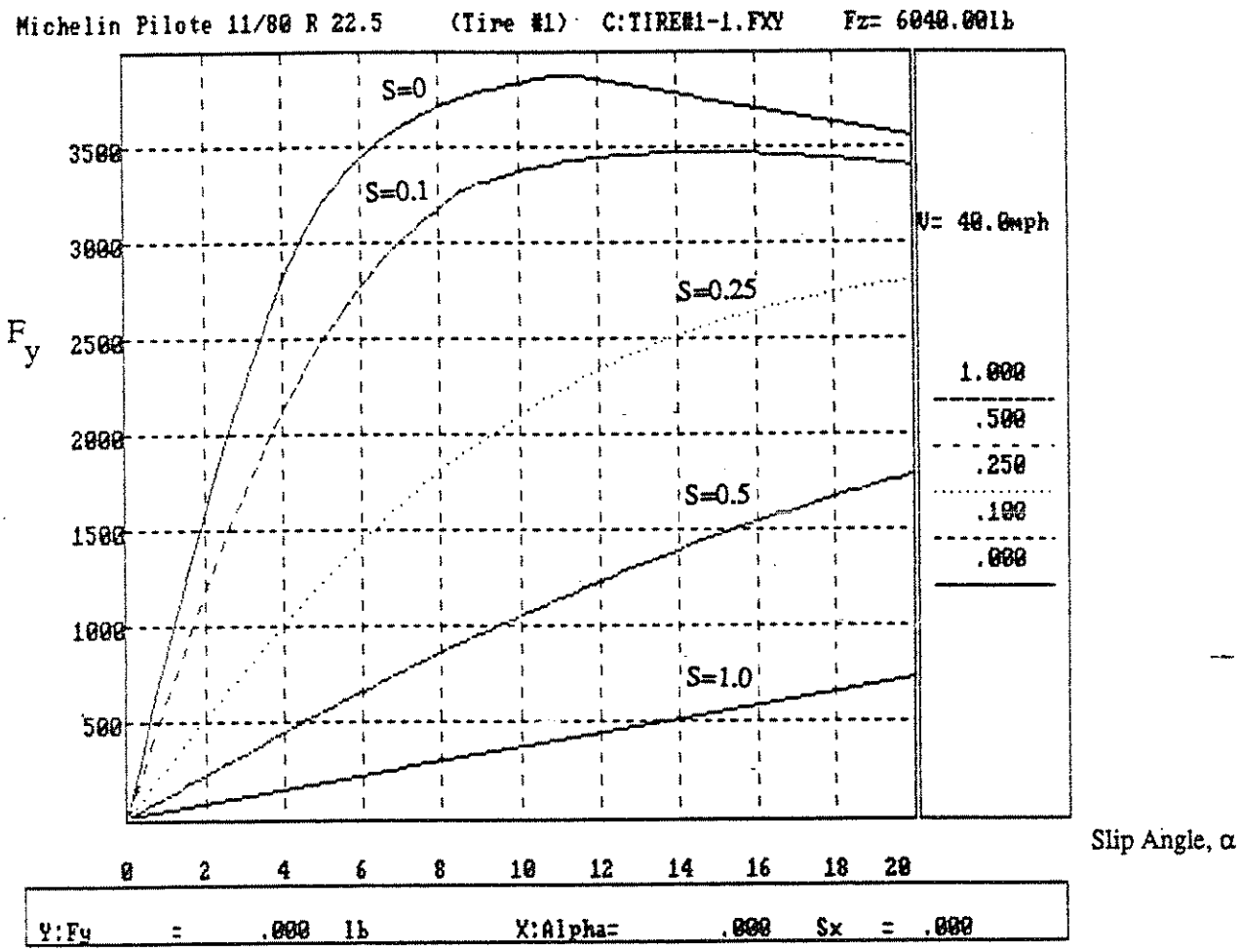

Figure 24. Lateral Force, F_y vs. Slip Angle, α, at different slips, s_x

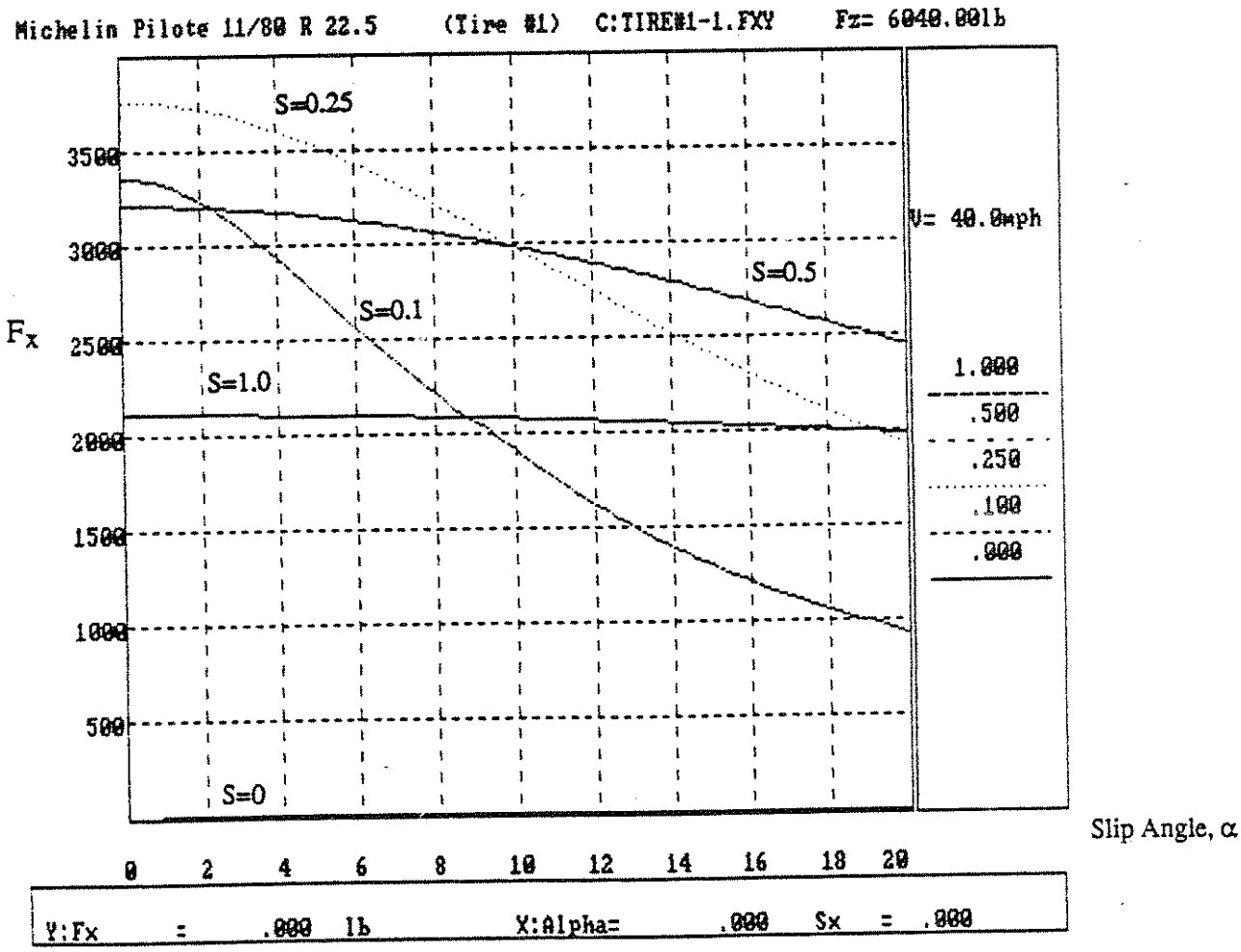

Figure 25. Longitudinal Force, F_x vs. Slip Angle, α, at different slips, s_x

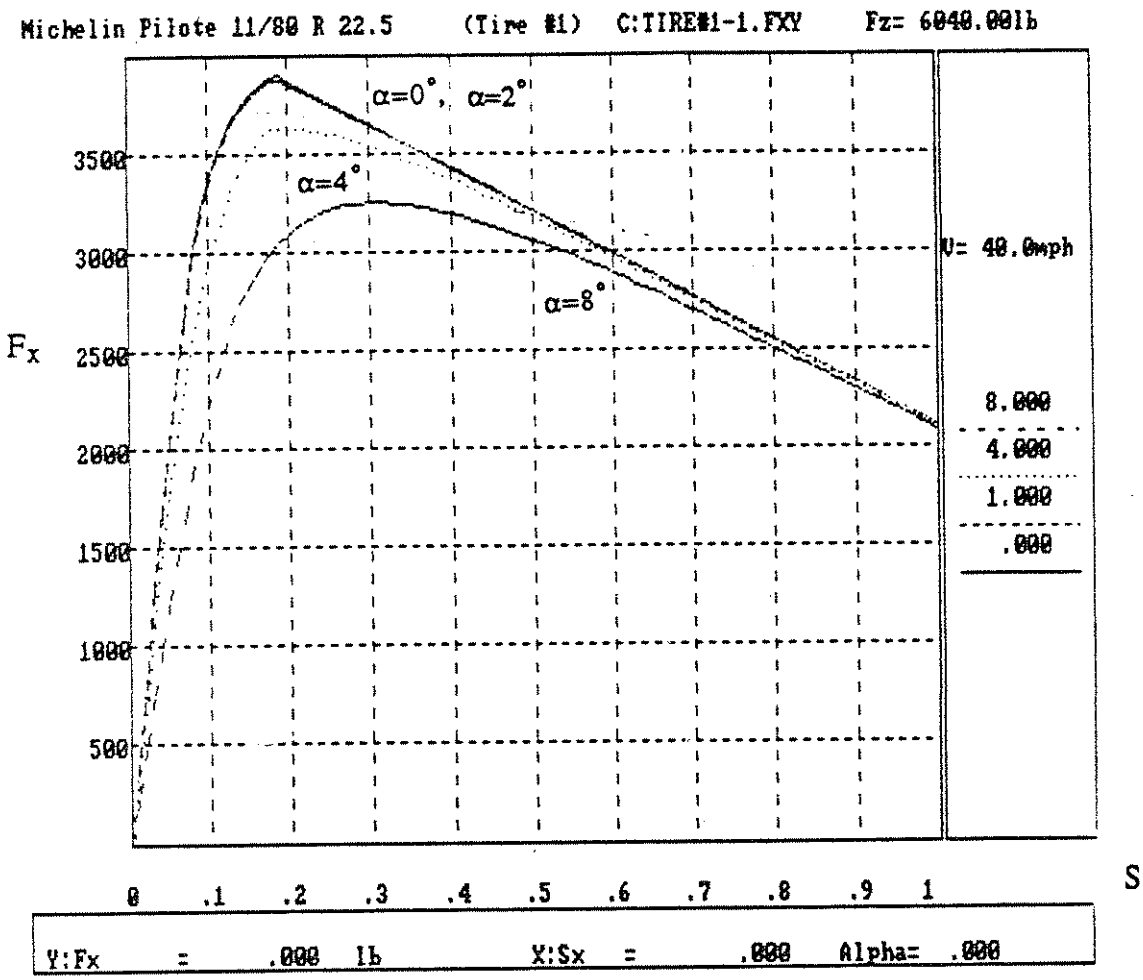

Figure 26. Longitudinal Force, F_x vs. slip, s_x, at different Slip Angles, α

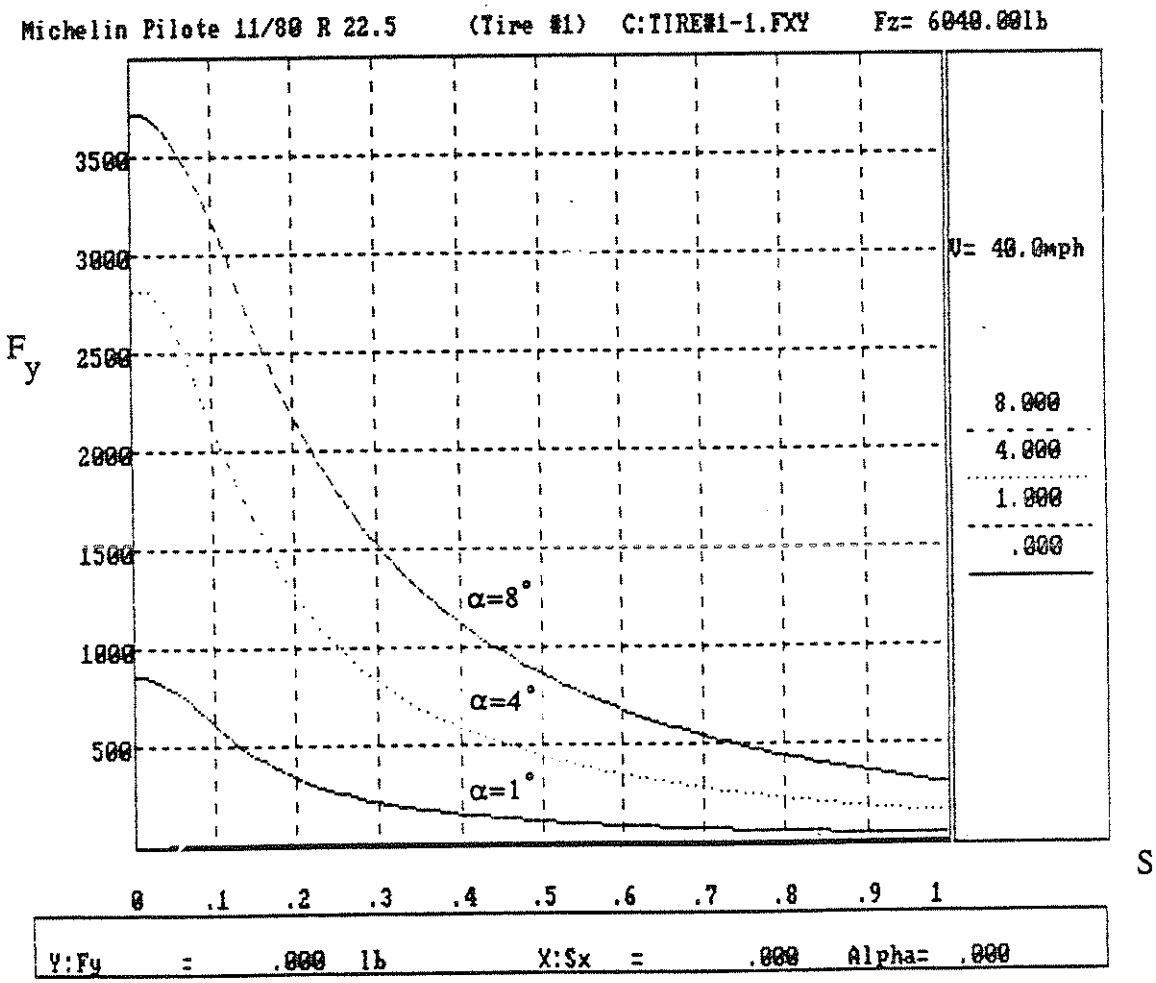

Figure 27. Lateral Force, F_y vs. slip, s_x, at different Slip Angles, α

influenced by slip angle but that the influence is modest up to levels of slip angle that correspond to conditions at which heavy trucks would be expected to roll over.

Figure 27 is the lateral force counterpart of Figure 25. In this case the curves are easy to interpret because they do not intersect for the ranges of slip angle considered. As in Figure 24, these curves show the dramatic effect of longitudinal slip on lateral force. The influences of the lateral parameters (C_α and a/L) are important at low levels of longitudinal slip, but their influences are greatly reduced as longitudinal slip increases and a large fraction of the contact patch is sliding.

5.0 CONCLUDING REMARKS

This study has included work investigating the details of the generation of lateral force. It has also included efforts to incorporate those details into a comprehensive model of traction fields. In order to use these results it is necessary to gather and process tire data with the model in mind. Certain types of essential data can be measured by flatbed and mobile dynamometers such as those employed by UMTRI. Figure 28 illustrates the sources of data that are convenient to use in estimating parameters for the tire model.

During the next fiscal year, UMTRI plans to address issues associated with friction levels pertaining to truck tires operating on wet roads. That effort will provide the basis for using the comprehensive tire model to predict traction fields on poor wet roads, for example. It will contribute to answering questions associated with the block labelled "friction decisions" in Figure 28.

Also, UMTRI has plans to upgrade its mobile dynamometer so that tire forces can be measured when the tire is subjected to both longitudinal and lateral slip. With this capability, it would be possible to make comparisons between model predictions and measured data under conditions of combined slip—something that has never been done before for truck tires. This would provide a good test of our understanding of the basic mechanisms determining tire shear force properties.

Finally, the analyses performed in this study show that including a nonuniform pressure distribution that changes shape as a function of vertical load represents a salient advancement in tire modeling.

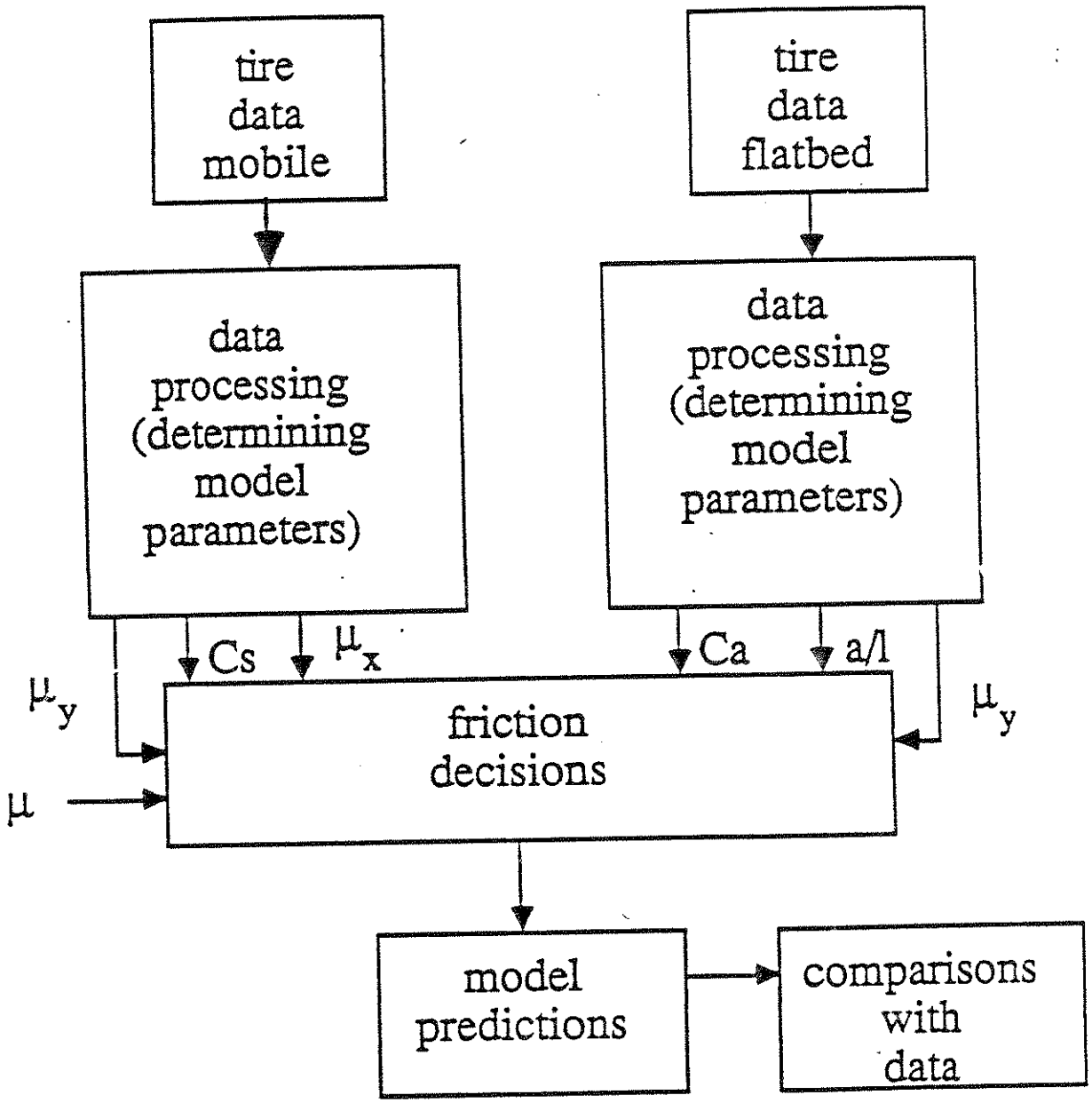

Figure 28. Tire Studies

REFERENCES

1. Olson, P.L., et al. "Parameters Affecting Stopping Sight Distance." Nat. Coop. Highway Res. Prog., Rept. 270, The Univ. of Mich., Transp. Res. Inst., June 1984.

2. Winkler, C.B., Fancher, P.S., and MacAdam, C.C. "Parametric Analysis of Heavy Duty Truck Dynamic Stability." Final Rept., Contract No. DTNH22-80-C-07344, The Univ. of Mich., Transp. Res. Inst., Rept. No. UMTRI-83-13, March 1983.

3. Fancher, P.S. and Mathew, A. "A Vehicle Dynamics Handbook for Single-Unit and Articulated Heavy Trucks." Final Rept., Contract No. DTNH22-83-C-07187, The Univ. of Mich., Transp. Res. Inst., Rept. No. UMTRI-86-37, May 1987.

4. Dugoff, H., Fancher, P., and Segel, L. "An Analysis of Tire Traction Properties and Their Influence on Vehicle Dynamic Performance." 1970 International Automobile Safety Conference Compendium, SAE Paper No. 700377, New York 1970.

5. Bernard, J.E., Segel, L., and Wild, R.E. "Tire Shear Force Generation During Combined Steering and Braking Maneuvers." SAE Paper No. 770852, 1977.

6. Press, W.H., et al. *Numerical Recipes, The Art of Scientific Computing*. Cambridge Univ. Press, 1986.

7. Tielking, J.T., Fancher, P.S., and Wild, R.E. "Mechanical Properties of Truck Tires." SAE Paper No. 730183, 1973.

APPENDIX A

TIRE MODEL FOR COMBINED STEERING AND BRAKING MANEUVERS

This appendix gives equations describing the semi-empirical tire model.

EQUATIONS

The frictional coupling between the road and the tire is defined as;

$$\mu = \mu_0 * (1 - A_S * V_S) \tag{1}$$

where:

$$V_S = u_W * \left[S_x^2 + \tan(\alpha)^2 \right]^{1/2} \tag{2}$$

$$\mu_0 = \mu_x + (\mu_y - \mu_x) * \frac{2}{\pi} * \theta \tag{3}$$

$$\theta = \tan^{-1}\left(\frac{\tan \alpha}{S_x}\right) \tag{4}$$

V_S is the sliding velocity, and μ_0 is the combined frictional coupling. θ is the angle between the sliding direction and the undeformed center line of the contact patch. Defining also λ as;

$$\lambda = \left[S_x^2 + \left(\frac{C_\alpha}{C_S} * \tan \alpha\right)^2 \right]^{1/2} \tag{5}$$

Using these definitions and after the integration we obtain for each pressure zone.

- **Case (1)**

Decreasing pressure zone, $L\text{-}a < x_s \leq L$. Sliding will occur when:

$$\frac{x_s}{L} = \frac{\mu * F_Z * (1 - S_x)}{\mu * F_Z * (1 - S_x) + 2 * C_S * \lambda\,(a/L) * (1 - a/L)} \tag{6}$$

$$F_X = \frac{C_S * S_x}{1 - S_x}\left(\frac{x_s}{L}\right)^2 + \frac{\mu * |F_Z| \cos\theta}{2 * (a/L) * (1 - a/L)}\left(1 - \frac{x_s}{L}\right)^2 \tag{7}$$

$$F_Y = \frac{C_\alpha * \tan\alpha}{1 - S_x}\left(\frac{x_s}{L}\right)^2 + \frac{\mu * |F_Z| \sin\theta}{2 * (a/L) * (1 - a/L)}\left(1 - \frac{x_s}{L}\right)^2 \tag{8}$$

- Case (2)

Central region of pressure distribution, $a < x_s \leq L\text{-}a$. Sliding will occur when:

$$\frac{x_s}{L} = \frac{\mu * F_Z * (1 - S_x)}{2 * C_S * \lambda * (1 - a/L)} \tag{9}$$

$$F_X = \frac{C_S * S_x}{1 - S_x}\left(\frac{x_s}{L}\right)^2 + \frac{\mu * |F_Z| \cos\theta}{(1 - a/L)}\left(1 - \frac{x_s}{L} - \frac{a}{2L}\right) \tag{10}$$

$$F_Y = \frac{C_\alpha * \tan\alpha}{1 - S_x}\left(\frac{x_s}{L}\right)^2 + \frac{\mu * |F_Z| \sin\theta}{(1 - a/L)}\left(1 - \frac{x_s}{L} - \frac{a}{2L}\right) \tag{11}$$

- Case (3)

Increasing pressure zone, $0.0 \leq x_s \leq a$. Sliding will occur at all points.

$$F_X = \mu * |F_Z| * \cos\theta \tag{12}$$

$$F_Y = \mu * |F_Z| * \sin\theta \tag{13}$$

ALIGNING TORQUE

The aligning torque is calculated as follows:

$$A_T = -F_y * X_P * \left(\frac{x_s}{L}\right) + F_y * F_X / C_y \tag{14}$$

ROLL-OFF TABLES

The roll-off tables are computed as follows:

$$\text{ROLL-}X_{\alpha,\, s_x} = \frac{F_{X_{\alpha, s_x}}}{F_{X_{\alpha=0, s_x}}} \tag{15}$$

$$\text{ROLL-}Y_{\alpha,\, s_x} = \frac{F_{Y_{\alpha, s_x}}}{F_{Y_{\alpha, s_x=0}}} \tag{16}$$

APPENDIX B

AN EXAMPLE OF PARAMETRIC INPUT AND NUMERICAL OUTPUT FOR A TRACTION FIELD

COMBINED TIRE MODEL

FILE NAME:C:TIRE#1-1.FXY

Date: 6-28-1988 Time:14:50: 6

Comment : Michelin Pilote 11/80 R 22.5 XZA (Tire #1)

Nominal Load = 6040.00 lb
Nominal Velocity = 40.000 MPH

Nominal Values of:

Cornering Stiffness, Calfa = 929.370 Lb/deg

Lateral Friction Coeff., Mu-y = .713900

Longitudinal Friction Coeff., Mu-x = .713900

Longitudinal Stiffness, Cs = 47190.9 Lb/unit slip

Pressure Distribution Parameter, a/l = .238200

Pneumatic Trail, Xp = 1.97940 inches

Lateral Deflection Stiffness, Cy = 4614.82 lb/in

Friction Reduction Factor, As = .870000E-02 sec/ft

Rate of Change and Curvature with Respect to Load

	Linear Coeff.	Quadratic Coeff.
Calfa :	.725000E-01	-.177600E-04
Mu-y :	-.224790E-04	.384600E-08
Mu-x :	-.224790E-04	-.384600E-08
Cs :	1.54350	-.581340E-03
a/l :	-.294220E-04	-.408200E-08
Xp :	.257160E-03	.150300E-08
Cy :	.000000	.000000
As :	.000000	.000000

Rate of Change and Curvature with Respect to Speed

	Linear Coeff.	Quadratic Coeff.
Calfa :	.000000	.000000
Mu-y :	.000000	.000000
Mu-x :	.000000	.000000
Cs :	-266.051	2.50400
a/l :	.000000	.000000
Xp :	.000000	.000000
Cy :	.000000	.000000
As :	.000000	.000000

COMBINED TIRE MODEL

FILE NAME:C:TIRE#1-1.FXY

Simulation Load = 6040.00 Lb
Simulation Velocity = 40.000 MPH

Alpha = .00

Sx	Fx (lb)	Fy (lb)	Alig. Torq. (in-lb)
.00	.00	.00	.00
.10	3356.01	.00	.00
.20	3871.78	.00	.00
.30	3651.69	.00	.00
.40	3431.61	.00	.00
.60	2991.43	.00	.00
.80	2551.26	.00	.00
1.00	2111.08	.00	.00

Alpha = 1.00

Sx	Fx (lb)	Fy (lb)	Alig. Torq. (in-lb)
.00	.00	861.47	-1580.44
.10	3324.63	609.94	-166.82
.20	3855.52	336.49	122.47
.30	3644.51	212.05	67.48
.40	3427.64	149.57	40.57
.60	2989.81	86.98	15.34
.80	2550.50	55.65	4.52
1.00	2110.76	36.84	-.52

Alpha = 2.00

Sx	Fx (lb)	Fy (lb)	Alig. Torq. (in-lb)
.00	.00	1603.92	-2738.44
.10	3234.89	1182.69	-283.02
.20	3807.79	664.85	235.11
.30	3623.18	421.75	132.27
.40	3415.80	298.21	80.12
.60	2984.95	173.73	30.46
.80	2548.23	111.23	8.98
1.00	2109.80	73.68	-1.05

Alpha = 4.00

Sx	Fx (lb)	Fy (lb)	Alig. Torq. (in-lb)
.00	.00	2807.95	-4074.06
.10	2931.51	2124.25	-321.56
.20	3631.24	1269.60	400.40
.30	3540.73	825.31	244.09
.40	3369.34	589.02	152.33
.60	2965.66	345.63	59.15
.80	2539.17	221.94	17.47
1.00	2105.94	147.26	-2.23

Alpha = 8.00

Sx	Fx (lb)	Fy (lb)	Alig. Torq. (in-lb)
.00	.00	3708.28	-2578.67
.10	2213.62	3176.37	-128.65
.20	3092.11	2172.84	431.41
.30	3250.88	1522.94	354.77
.40	3196.38	1123.05	248.35
.60	2890.65	677.09	104.88
.80	2503.36	439.78	31.21
1.00	2090.54	293.81	-5.43

Alpha = 10.00

Sx	Fx (lb)	Fy (lb)	Alig. Torq. (in-lb)
.00	.00	3835.62	-2085.63
.10	1910.42	3368.58	-193.76
.20	2800.93	2469.40	334.48
.30	3067.17	1802.75	348.19
.40	3078.63	1357.12	265.49
.60	2836.55	833.60	119.34
.80	2476.94	545.94	35.62
1.00	2079.01	366.59	-7.69

Alpha = 12.00

Sx	Fx (lb)	Fy (lb)	Alig. Torq. (in-lb)
.00	.00	3854.37	-1817.31
.10	1620.34	3444.14	-414.59
.20	2524.29	2682.77	202.56
.30	2872.52	2035.24	307.24
.40	2946.62	1565.81	261.52
.60	2772.78	982.29	127.06
.80	2445.15	649.66	37.91
1.00	2064.95	438.92	-10.55

Alpha = 16.00

Sx	Fx (lb)	Fy (lb)	Alig. Torq. (in-lb)
.00	.00	3705.31	-1747.03
.10	1208.33	3464.83	-726.42
.20	2043.64	2930.03	-83.94
.30	2482.41	2372.73	157.62
.40	2658.26	1905.61	199.20
.60	2621.13	1252.66	120.87
.80	2366.60	848.26	35.06
1.00	2029.30	581.89	-18.48

Mu-x Roll-Off Table

Longitudinal Slip, Sx

Alpha	.00	.10	.20	.30	.40	.60	.80	1.00
.00	1.000	1.000	1.000	1.000	1.000	1.000	1.000	1.000
1.00	1.000	.991	.996	.998	.999	.999	1.000	1.000
2.00	1.000	.964	.983	.992	.995	.998	.999	.999
4.00	1.000	.874	.938	.970	.982	.991	.995	.998
8.00	1.000	.660	.799	.890	.931	.966	.981	.990
10.00	1.000	.569	.723	.840	.897	.948	.971	.985
12.00	1.000	.483	.652	.787	.859	.927	.958	.978
16.00	1.000	.360	.528	.680	.775	.876	.928	.961

Mu-y Roll-Off Table

Longitudinal Slip, Sx

Alpha	.00	.10	.20	.30	.40	.60	.80	1.00
.00	1.000	1.000	1.000	1.000	1.000	1.000	1.000	1.000
1.00	1.000	.708	.391	.246	.174	.101	.065	.043
2.00	1.000	.737	.415	.263	.186	.108	.069	.046
4.00	1.000	.757	.452	.294	.210	.123	.079	.052
8.00	1.000	.857	.586	.411	.303	.183	.119	.079
10.00	1.000	.878	.644	.470	.354	.217	.142	.096
12.00	1.000	.894	.696	.528	.406	.255	.169	.114
16.00	1.000	.935	.791	.640	.514	.338	.229	.157